UNIVERSITEIT GENT

FACULTEIT GENEESKUNDE EN GEZONDHEIDSWETENSCHAPPEN

Academiejaar 2010 - 2011

Magnetic Resonance Spectroscopy in Normal Aging and Mild Cognitive Impairment: Quantitative and methodological aspects

Tom Claeys

Promotor: Prof. Dr.E. Achten
Co-promotor: Prof. Dr. P. Santens

Scriptie voorgedragen in de 2de Master in het kader van de opleiding tot
MASTER IN DE GENEESKUNDE

Preface

"There is nothing like looking, if you want to find something. You certainly usually find something, if you look, but it is not always quite the something you were after."

- J.R.R. Tolkien -

This thesis is the result of personal study and cooperation with the Ghent Institute for functional and Metabolic Imaging of the brain (GIfMI), which is connected to Ghent University. I would like to use this opportunity to thank several people who helped and guided me during this period. Firstly, my sincerest thanks go out to Prof. dr. E. Achten and Prof. dr. P. Santens, respectively promotor and co-promotor of this thesis, for giving me this chance and introducing me to experimental research. To all researchers at the GIfMI, for their time and guidance during my research. Also to Leslie Vlerick, for his assistance and company during scanning sessions. And special thanks go out to Harmen Reyngoudt, for his unlimited patience, great wit and infinite knowledge in guiding me trough this process.

Tom Claeys.

Contents

Abstract

^{1}H-MR spectroscopy (^{1}H-MRS) started as an in vitro chemical analytic method. Now it provides for physiopathological insights in in vivo neurological and psychological research. In this thesis ^{1}H-MRS is used in unraveling physiological mechanisms behind aging and cognitive impairment. It allows for measurements of metabolite ratios and absolute metabolite concentrations in brain areas that are involved in cognitive decline, such as the posterior cingulated cortex (PCC) and the hippocampus (HC). The NOMARED study researched the physiology of normal aging in 90 healthy subjects. The MCI study searched for differences between 6 healthy control subjects and 8 Mild Cognitive Impaired (MCI) patients. 10 healthy young adults were examined in the NOMAREDplus study to determine T_1 and T_2 metabolite relaxation times, as well as to clarify the evolution of cerebrospinal fluid (CSF) fraction with age.

Results showed that normal aging correlates with a possible gliosis in the PCC. This was concluded from significant (P<0.05) age-related increases in myo-inositol (Ins) and total creatine (tCr), and a concomitant trend (P=0.097) in decreasing N-acetylaspartate/total creatine ratio (NAA/tCr) with age. In the HC only significant increases of Ins were found. Aging also appears to be associated with a decrease in neuronal cell volume, rather than with a fall in cell numbers. This was shown by a trend (P=0.072) in increasing absolute NAA concentration with age.

Furthermore, this study showed CSF fractions to increase with age (P<0.001). When including results of the NOMAREDplus study, CSF fractions appeared to decrease to a minimum during young adulthood. This decline was followed by a steady increase during further aging, which could imply that some aspects of aging do not start at birth, but later in life.

Finally, pathological aging in MCI patients might be related to membrane lipid breakdown, which is reflected in increased choline (Cho) levels. In normal subjects an age-related fall in Cho/tCr ratio was found, whereas in MCI patients raised absolute Cho concentrations were seen compared to normal subjects (*P=0.08)*.

Abstract (Dutch)

^{1}H-MR spectroscopie (^{1}H-MRS) werd vooreerst gebruikt bij in vitro chemische analyses, maar biedt nu ook pathofysiologische inzichten bij in vivo neurologisch en psychologisch onderzoek. In deze thesis wordt deze techniek aangewend om fysiologische mechanismen van veroudering en cognitieve achteruitgang te ontwaren. Het laat toe om metabolietenratios en absolute metabolietenconcentraties te meten in regio's die betrokken zijn bij cognitieve achteruitgang, zoals de posterieur cingulaire cortex (PCC) en de hippocampus (HC). In de NOMARED studie werd het proces van normale veroudering onderzocht bij 90 gezonde proefpersonen. De MCI studie vergeleek 6 gezonde proefpersonen met 8 mild cognitief berperkte (MCI) patiënten. Data van 10 gezonde, jonge volwassenen werd in de NOMAREDplus studie aangewend om de T_1 en T_2 relaxatietijden van metabolieten te bepalen, alsook om de veranderingen in cerebrospinaal vocht (CSV) gehalte verder in kaart te brengen.

De resultaten toonden aan dat normale verouderingsprocessen gepaard gaan met een mogelijke gliose in de PCC. Deze gliose uitte zich in een significante (P<0.05), leeftijdsgebonden stijging van myo-inositol (Ins) en totaal creatine (tCr), alsook in een concomitante daling van de ratio N-acetylaspartaat/totaal creatine (NAA/tCr) (P=0.097). In de HC werd enkel een significante stijging van Ins gevonden.
Veroudering lijkt tevens gepaard te gaan met een daling van het neuronaal celvolume en niet zozeer met een daling in het aantal neuronen. Dit werd geconcludeerd uit een niet-significante (P=0.072) daling van de absolute NAA concentratie bij het verouderen.
Verder bleek de fractie CSV in de hersenen af te nemen bij veroudering (P<0.001). Wanneer de resultaten van de NOMAREDplus studie toegevoegd werden, bleek de relatieve CSV inhoud in de hersenen af te nemen tot in de vroege volwassenheid. Vervolgens nam deze CSV inhoud weer toe, wat er kan op wijzen dat bepaalde aspecten van veroudering niet vanaf de geboorte starten, maar pas later in het leven.
Tenslotte leek de pathologische veroudering in MCI patiënten gepaard te gaan met een verhoogde afbraak van membraanlipiden, hetgeen zich uitte in verhoogde Cho concentraties. Bij normale proefpersonen werd een leeftijdsgebonden afname van de Cho/tCr ratio gevonden, terwijl bij MCI patiënten de absolute Cho concentratie verhoogd was in vergelijking met normale proefpersonen (P=0.08).

Introduction

Magnetic Resonance

Magnetic Resonance is generally known as a method of non-invasive, detailed anatomical imaging, used in medical practice and research. There are however, a myriad of other usages of this technology, such as Magnetic Resonance Spectroscopy (MRS). This technique was first introduced as a chemical analytic method in order to identify molecules by their biophysical properties. In the clinic it provides an opportunity to study small metabolites *in vivo*, typically in concentrations of 0.5-10 mM. This offers unique insights to metabolic pathways or changes in normal physiology, as well as in pathology. Most frequently used MRS applications are situated in the fields of neurology, infectiology, traumatology, and oncology, due to the sensitivity of the technology for soft tissue parts of the body. (1)

Hardware

The required hardware consists of a large magnetic bore that creates the static magnetic field B_0, a radio frequent RF-coil creating a time-varying magnetic field B_1 and gradient coils that allow for the selection of a volume of interest (VOI) by means of three-dimensional magnetic field gradients. During past decades MR systems were produced with magnetic field strengths from 1.5T, 3T, and even up to 11.7T. This was accomplished by the introduction of superconductive coils and the use of cryogenic coolants, such as liquefied helium. Such increases brought forward major improvements in resolution, but also a steady rise in costs. RF coils are needed for transmitting and receiving RF signals. These can be integrated in a single transmit-receive component, or may consist of separate modules. Further improvements in MR systems were made in coil design, thus also increasing sensitivity of MR systems. (1, 2)

Physiological information is obtained by producing MR spectra of different metabolites, by using nuclei such as, ^{1}H, ^{31}P, ^{19}F and ^{23}Na. In medicine, however, the ^{1}H nucleus is the most widely used in MRS, because of its presence in most metabolites. Furthermore, the ^{1}H signal in soft tissue is used for anatomical imaging, so the same RF coils may be used for MRI as for ^{1}H MRS.

MR Physics

A brief introduction to basic MR physics follows in the next sections.

Human bodies consists mainly out of water, comprising hydrogen and oxygen atoms. The hydrogen nucleus consists of a single proton that revolves around its own axis. A rotating proton with an electrical charge generates a magnetic field, inducing a magnetic dipole moment. These nuclei can be perceived as small bar magnets. (see fig. 1)

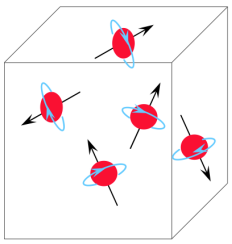

Figure 1 Protons as bipolar magnets.

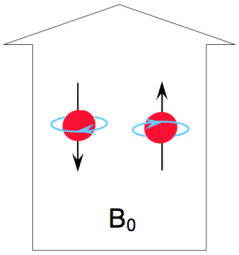

Figure 2 Protons in external magnetic field.

Upon placement of these protons in an external magnetic field, two main phenomena occur. Firstly the protons orient themselves parallel or anti-parallel to the imposed field, along the direction of the B_0 field. (see fig. 2) There is a slight advantage in the parallel oriented protons, depending on the magnetic field strength (eg. 0,5T 3ppm more for the parallel orientation, 1,5T 9ppm). (2) This net difference is used for signal readings and is often represented as a vector. This explains the increase in image quality by using higher field strengths.

Secondly, protons in a magnetic field undergo a precession movement, much like a spinning top. This movement is subject to a steady frequency, called the Larmor frequency: $\omega_0 = \gamma.B_0$, in which γ represents the element specific gyromagnetic ratio. (eg. Larmor frequency hydrogen in 3T system: 3 T. 42,57 MHz/T = 127,71 MHz).

During data acquisition a radio frequent pulse (RF pulse) is broadcasted at this Larmor frequency, with certain amplitude and duration. This triggers a rotation of the net magnetization away from the *Z*-axis, with a varying flip angle between 1 and 180 degrees (eg. 90 degree flip angles encompasses the *XY*-plane). This phenomenon is called excitation. (see fig. 3) After the cessation of this RF pulse, relaxation to the former state sets in, which can be divided in spin-lattice and spin-spin relaxation. The spin reflects the intrinsic physical property of nuclei.

Spin lattice is a phenomenon in which a part of the excitation energy is dissipated back into the environment, characterized by the spin-lattice or T_1 relaxation time. The T_1 value reflects the time needed for the *Z*-component of the magnetization to recover 63% of its initial value following RF excitation. This varies for each molecule, among other reasons, due to specific proton compositions. (see fig. 3, 4 and 5)

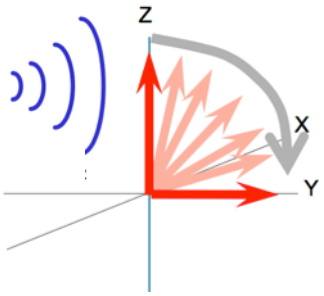

Figure 3 Excitation.

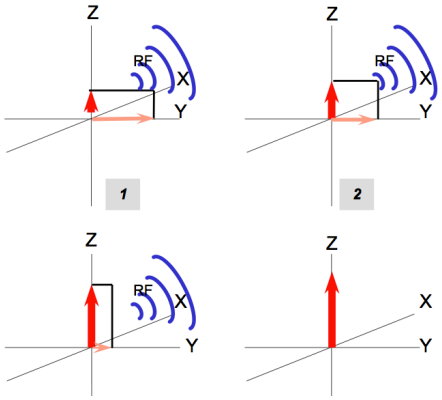

Figure 4 T_1 relaxation.

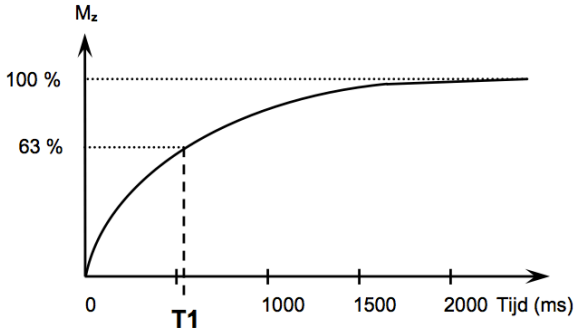

Figure 5 T_1 relaxation signal.

Spin-spin relaxation is a phenomenon in which energy is exchanged between spins or protons themselves, characterized by the spin-spin or T_2 relaxation time. Following the RF pulse the components are phased, resulting in a large vector. This vector reduces in size, due to loss of coherence in spins, called dephasing. This phase coherence disappears with a time constant T_2, due to magnetic field inhomogenities. The T_2 value reflects the time needed for the transverse component of the magnetization to decay to 37% of its initial value following RF excitation. In general T_2 relaxation occurs at a higher rate than T_2 relaxation. (see fig. 6 and 7)

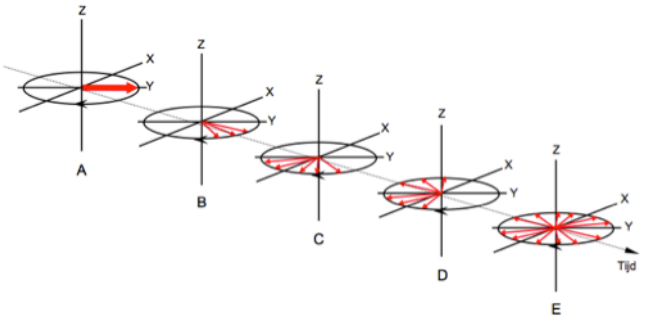

Figure 6 T2 relaxation.

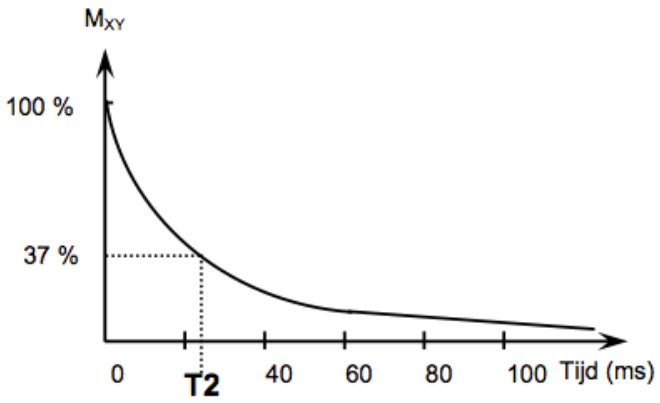

Figure 7 T2 relaxation curve.

During these relaxation processes, protons release the energy absorbed from the RF pulse, by means of radio frequent waves. Reception coils that are placed perpendicular to the main magnetic field, acquire these signals so that minute changes in B_0 can easily be differentiated.

Localization

Localization is an ingenious process wherein gradient magnetic fields are applied to the subject. A difference in magnetic field strength implies a slightly different Larmor frequency. By imposing a gradient along the *Z*-axis axial slices are selected. Along the *Y*-axis phase coding is used: a magnetic gradient triggers a difference in phase, thus creating a anterior-posterior difference. The voxel of interest (VOI) is determined by a final *X*-magnetic gradient that distinguishes between left and right. Online processing of many voxels, eg by means of Fourier analysis, leads to imaging and/or specific readings, such as MRS spectra.

Pulse sequences

The needed broadcast signal comprises several events (RF pulse, gradient shifts en signal reception) and is called a pulse sequence. (see fig. 8)

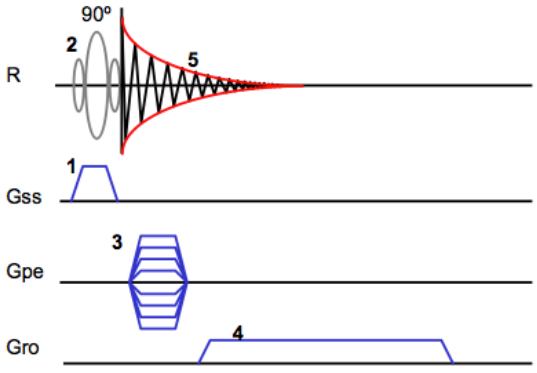

Figure 8 Pulse sequence: R = Radiofreqruent Pulse + Free induction Decay (FID) signal; Gss = slice select gradient at same time as RF pulse; Gpe = phase encoding gradient; Gro= read out gradient during FID signal.

A frequently applied sequence is the Spin Echo Sequence. After a 90-degree flip angle excitation pulse, spin-spin relaxation occurs (FID FreeInduction Decay). However, protons in phase give out a stronger signal. In order to keep phase coherence, a second RF pulse is given, a 180-degree pulse, which rephases all protons and safeguards the signal intensity. Following analogy may clarify: track runners disperse after take off (dephasing). After 20 seconds the fastest one has a certain advantage over the slowest. The runners are now instructed to stop, turn and head back at the same speed at the blow of a whistle (eg. After 20 seconds). The fastest runner is now behind on the slowest, but after another 20 seconds, they will all have reached their same starting point (rephasing). (3) (see fig. 9) This second signal slowly increases and gives rise to an echo. (see fig. 10) The obvious advantage is an increase in signal strength, but on the down side, an extra pulse causes longer scanning times and extra exposure to RF waves.

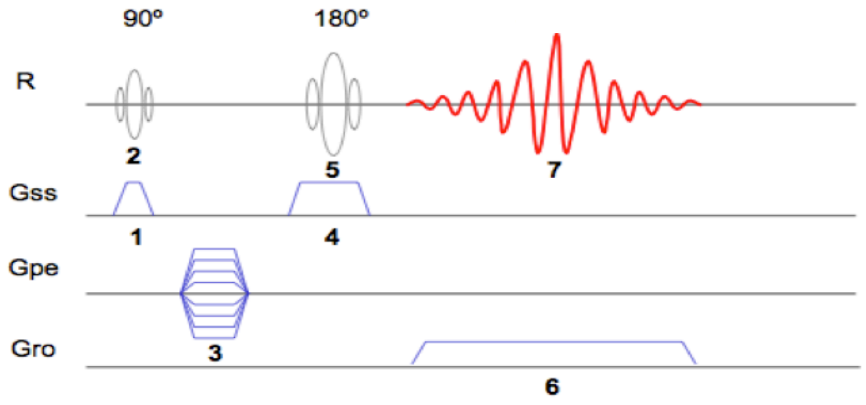

Figure 9 Pulse sequence with 180-degree pulse.

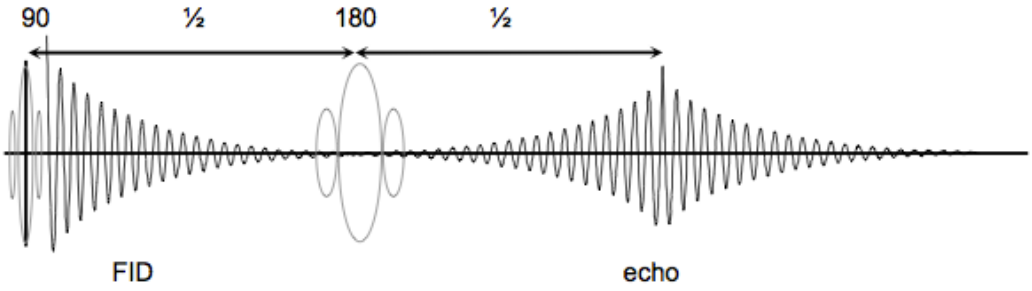

Figure 10 Signal with FID and Echo.

This allows for the introduction of some basic concepts in MR. *TR*, repetition time is the time between two 90-degree pulses. *TE*, echo time, is the time between 90 degree excitation pulse and the echo read out. (see fig. 11)

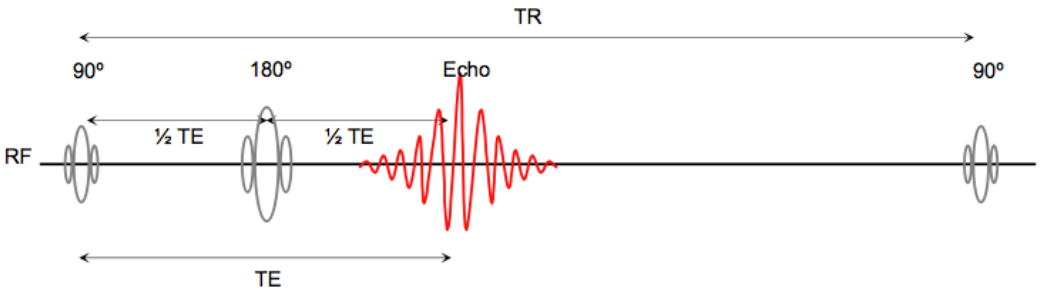

Figure 11 Signal concepts.

Single voxel ^{1}H MR Spectroscopy mainly uses point-resolved spectroscopy sequences (PRESS) or stimulate echo acquisition mode sequences (STEAM). Both use a three-pulse sequence (see fig. 12), combined with a *X-, Y-* and *Z*-gradient for localization purposes. For quantitative measurements, a short *TE* with long *TR* is preferred with minimal signal loss. Longer *TE* provides for sharper defined spectral peaks that are more easily quantified. Because of better Signal to Noise Ratio (SNR), PRESS sequences have become the most popular in ^{1}H MRS. (1).

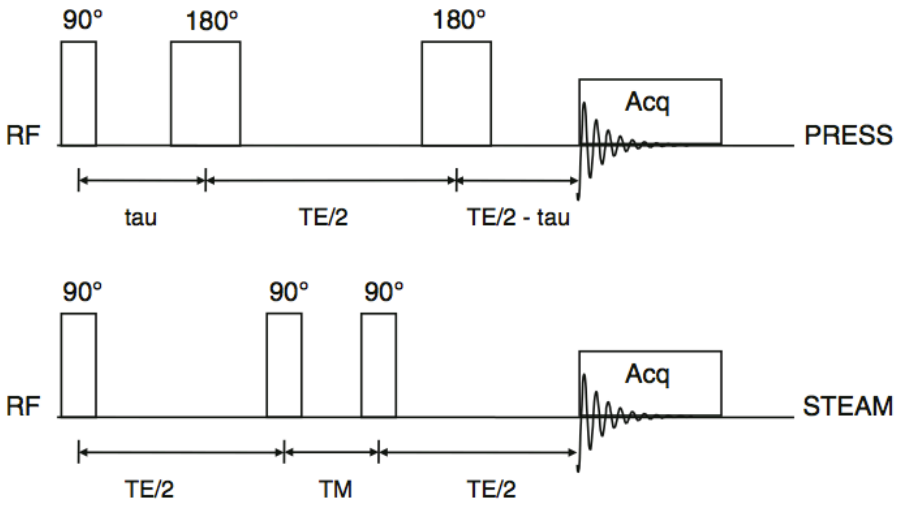

Figure 12 Press and STEAM sequences for MRS. RF = radio frequent pulse; tau = time delay between 90- and 180-degree pulses; TM = mixing time.

T_1 versus T_2 weighted images

MR images can be either T_1 weighted images, or T_2 weighted.

A T_1 weighted image measures a high T_1 signal, without interference of T_2 relaxation. By using a short *TE* (eg 10ms) dephasing in the *XY*-plane has hardly begun. After the *TR* is reached (eg. 600ms) not all tissues have undergone complete T_1 relaxation. Eg. fatty tissues have undergone more T_1 relaxation than spinal fluid. During the next excitation pulse, the remaining fluid vector to be rotated is small, resulting in a smaller signal. This results in a T_1 weighted contrast image. (see fig. 13) (2)

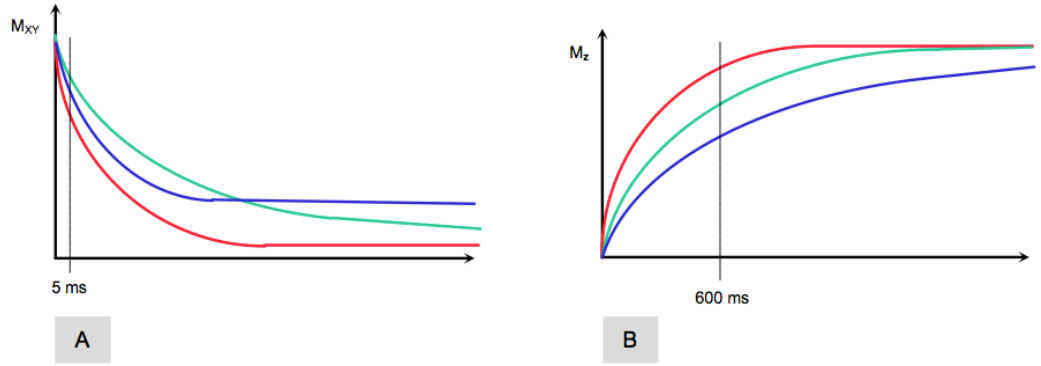

Figure 13 T1 weighted images, Signal intensity: green = grey matter; blue = liquor; red = fat. T_2 relaxation is observed before 5ms, in fig A; T_1 relaxation is observed at 600 ms, in fig B. Dephasing is barely noticeable in fig A, little T_2 contrast. T_1 relaxation is not yet complete for all tissues and creates T_1 contrast**.**

T_2 weighted images opt for the alternate: hereby the effect of T_2 relaxation is studied, and that of T_1 relaxation is disregarded. By using a longer *TE* (eg. 120ms) contrast between different tissues can be measured. A very long *TR* (eg. 3000ms) ensures that every proton reaches the same T_1 relaxation, thus not interfering with the signal. (see sig. 14)

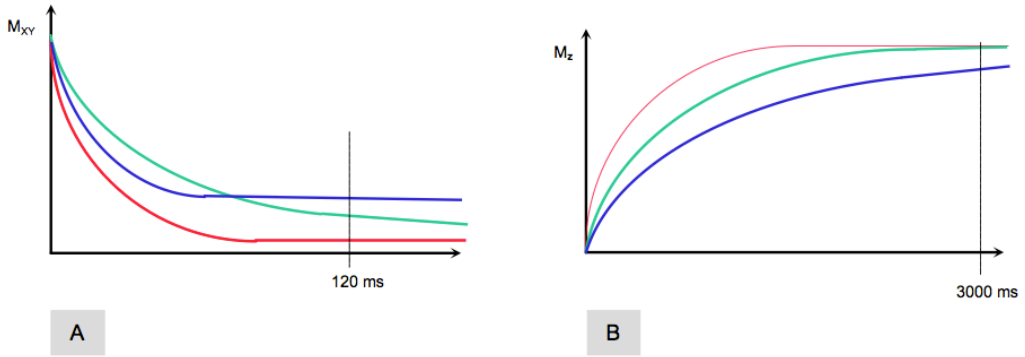

Figure 14 T2 weighted image, signal intensity: green = grey matter; blue = liquor; red = fat. T_2 relaxation is observed at 120 ms, in fig A; T_1 relaxation is observed at 300 ms, in fig B. Dephasing is noticeable in fig A, providing for T_2 contrast. T_1 relaxation is complete for all tissues and creates little T_1 contrast.

Chemical shift

Electrons of atoms placed in a magnetic field, will circulate themselves and cause a small magnetic field, opposing to the external field. The effective field at the nucleus is thus reduced. Since every nucleus in a molecule is surrounded by a different set of electrons with varying density, the opposing field at each nucleus will differ. This phenomenon is called chemical shift. It entails that every nucleus has a specific effective field and resonance frequency, which empowers us to identify separate nuclei.

This difference in resonance frequency depends on the externally applied field strength: the greater the field strength, the greater the difference. This also explains why high tesla equipment provides for better and more detailed imaging.

The chemical shift of a nucleus is the difference between the resonance frequency of the particular nucleus ν and that of a standard ν_{ref}, relative to the standard. It is reported in ppm and represented by δ. (see formula 1) Often tetramethylsilane (TMS) is used as a standard. For example the chemical shift difference between two common substances, fat and water, is circa 3,5 ppm. The biochemical fingerprint of important metabolites is well known. (table 1) (4)

$$\delta = \frac{\nu - \nu_{ref}}{\nu_{ref}} \bullet 10^6$$

Formula 1 Chemical shift as a difference in resonance frequencies, relative to a standard.

Brain Metabolite	Chemical shift (in ppm)
N-acetylaspartate (NAA_1)	2.02
N-acetylaspartate (NAA_2)	2.6
N-acetylaspartate (NAA_3)	2.5
Creatine (Cr)	3.03
Choline (Cho)	3.22
Myo-inositol (mI_1 or Ins_1)	3.56
Myo-inositol (mI_2 or Ins_2)	4.06
Glutamine and Glutamate (Glx)	3.65-3.8

Table 1 Chemical shift of selected brain metabolites.

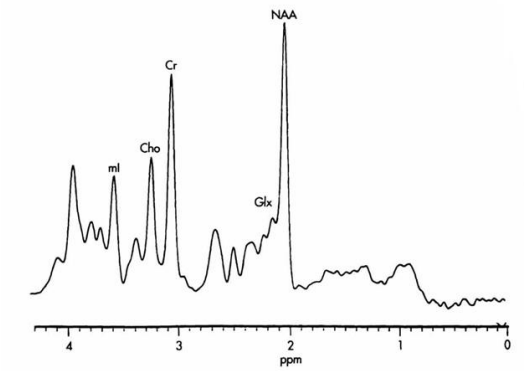

Figure 15 MR spectrum depicting Chemical Shift Phenomenon.

Voxel for MRS

MRS acquisition starts out with anatomical imaging, in which the volume of interest (VOI) is targeted by a voxel. This image is used as a spatial map of the scanner for further data acquisition, therefore it is crucial that the subject remains still during the ongoing examination.

Safety

In working with strong magnetic fields, safety is always a major concern. No harmful physiological effects are known to be caused by the field itself, but it does attract ferromagnetic objects. The danger lies in implants, or electronic devices that could be presented alongside the patient (e.g. pacemakers, defibrillators, aneurysm clips, orthopedic implants, orthodontics, cochlear implants, metal splinters, etc.). These should be checked for MR safety before scanning. Lately several MR compatible devices have become available, which can be checked online. (5) Loose metal objects can become projectiles in the presence of the scanner, so should therefore be avoided in the scanning room. Watches, credit cards and electronic devices can also be damaged by the magnetic field. Acoustic ear protection is needed to protect against the noise produced by the switching field gradients. These switching gradients may also cause slight nerve twitching for which the patient should be warned and monitored. Slight heating may occur during the scanning process. The cause of this, energy absorption is monitored by means of the Specific Absorption Rate (SAR). A SAR value of 1 Wkg^{-1} applied for one hour correlates with a temperature rise of 1°C. Pregnancy is not an absolute contraindication, but during first term pregnancies it is not advised to perform a scan. The main issue concerning MR systems is claustrophobia. Patients suffering from this, or people who can't succeed in lying still, may be sedated during the examination. (1)

Aging

Aging is a process that is easily recognized subconsciously, but is hard to define in a clear and noncontroversial way. Typically it is defined as " a progressive, unfavorable loss of adaptation resulting in decreasing expectation of life with the passage of time". This merely states that the older one gets, the closer one is to death; thus not even differentiating aging as a normal physiological process from specific pathological degenerative diseases. A definition of normal should meet following criteria: "First it should be universal, found in any individual that lives sufficiently long, secondly it should be intrinsic, not related to dietary or environmental factors, and it should be progressive." When considering these criteria in the search of a correct definition, the question remains whether aging should be defined as a functional or rather as an anatomical process. (6)

Physiology of aging

From an anatomical and physiological view several age-related changes have been unraveled in the human brain.

An early observation was brain atrophy in aging, which was first determined by means of autopsy. Among neurologically normal individuals a loss of brain weight of 2 to 3 grams per year, for an average brain of 1250 -1400 grams, was observed, which was largely attributed to losses in frontal lobes. A complicating factor was the "secular effect", which describes the increasing mean body height and brain weight during last century. A solution was found in the use of brain- to intracranial volume ratios and the assessment of sulcal widening and of ventricular enlargement in aging. This brain-to-intracranial-volume ratio appeared to remain fairly constant up to the age of 60 before reducing. This observation, as well as the progressive increase in ventricular volume was later confirmed by imaging studies. (6) Due to these findings, some studies estimated neural loss as high as 35%. However, this loss is largely attributed to changes in cell size, rather than neuronal cell number, leading to a constant neural density. (7)

Some studies have reported white matter changes that are correlated to normal cognitive impairment. They suggest that disruption of white matter tracts is consistent with cortical disconnection. (8)

Vascular changes have also been put forward as part of the aging mechanism. With age, arterio- and atherosclerotic changes increase in number throughout the body and the brain. This results in arterial tortuosities which are not related to systemic hypertension. (9) Furthermore, positron emission tomography (PET) studies have demonstrated a gradual decrease of cerebral blood flow and metabolism in frontal and parietal cortices. (10)

Glial changes have also been reported in normal aging, as an increase in both astrocytes (11) and microglial cells. The latter comprises solely enlarged and phagocytic forms, which correlate with higher tissue levels of interleukin-1. (12)

The deposition of several neural pigments has also been observed. Lipofuscin is an intracellular pigment that accumulates progressively in lysosomes, rather diffusedly in the brain. Neuromelanin accumulates, as a byproduct of catecholamine synthesis, in brainstem nuclei as the substantia nigra and locus coeruleus until the age of 60, but reduces after that. This results in a peroxidase-positive granule deposition, a process that is sped up in the presence of estrogen. (13)

Some have put forward a mitochondrial, metabolic aspect of aging. With age a smaller number of enlarged mitochondria remains with reduced metabolic efficiency. These changes correlate with a decreased functional ATP reserve and relative increase in free radical production, which reduces cellular capacity to oppose metabolic stressors. (14)

^{1}H-MRS in aging

During the last 15 years, the effect of age on metabolism has been studied on several occasions using ^{1}H-MRS, as shown in table 2. The age of subjects was correlated with ratios or absolute concentrations of proton metabolites. A large variability in results was found in all previous studies, partly due to different inclusion criteria (size, age range, medical history), regions of interest, data acquisition (field strength, single voxel versus multiple voxel studies, spectroscopy sequence, repetition time, echo time) and data processing (relative versus absolute quantification, correction factors). A decreased amount of N-acetylaspertate (NAA) with increasing age was observed in frontal (15, 16, 17, 18, 19, 20, 21), parietal (16, 17, 21) and temporal cortices (17, 22, 23, 24), and more specific regions such as, the sensorimotor cortex (25), the lentiform nucleus (21, 26), the caudate nucleus (21) and the supraventricular region (24). In contrast, some of these aforementioned studies did not find age-related NAA changes in the frontal cortex (25, 26) nor in the parietal cortex (25). Moreover, an increased NAA content with age has been observed in both the frontal and parietal cortex (27, 28). In several studies, an age-related increase in total creatine (tCr) was found in frontal white matter (15, 17, 21, 27, 28, 29) and parietal white matter (17, 27, 28, 29, 30, 31) . Similarly, choline (Cho) was also observed to increase with age in frontal white matter (15, 17, 21, 29), parietal white matter (17, 29, 31) and the temporal lobe (17). In a small number of studies, an increased amount of myo-inositol (Ins) was found in frontal (15, 21, 24) and parietal white matter (21, 24). One study reports variable age-related differences in γ-aminobutyric acid (GABA) and lactate (Lac) in dorsolateral prefrontal cortex, orbitofrontal cortex and sensorimotor cortex (25).

Aging: specific losses or a general reduction in function?

Of course the question remains whether aging and its effects on cognitive processes have a common cause or are rather a case of specific gain and loss in certain areas. A relevant example of the common-cause theory is the global-speed hypothesis. It assumes that aging generically speeds up or slows down cognitive processes, more so than its individual componential tasks. Specific-gain/loss theories, such as the neurocognitive-change hypothesis or the frontal-lobe hypothesis, perceive aging as a breakdown of separate structural and functional components of cognition. The frontal-lobe hypothesis for example, predicts age-related changes in executive tasks that are controlled in the frontal lobes, to be more pronounced than others. (32)

In a comparative study between these two models, Span et al found that the transition from childhood to adolescence and adulthood is triggered by a global processing speed change throughout both executive and non-executive tasks, thus supporting the common-cause theory. However, the transition into seniority could not solely be explained by this effect. Executive functions seem to deteriorate faster, so specific losses were also put forward as probable cause. “A global mechanism may account for large proportions of age-related variance in the speed of responding, process-specific changes in cognitive efficiency do occur”. (32) Further investigation into these specific changes and their causative factors is therefore needed.

Concluding, aging can described as a diverse process and is associated with a progressive, yet variable, decline of cognitive functions. (32)

Study	Size (M/F)[a]	Age range	Regions of interest[c]	B_0 (T)	MRS (I)	Quantification[d]	Results[g]
Chang et al. (1996) (15)	36	19-78	Frontal WM	1.5	MRS	A (EWR) + R	tCrt ↑ ,Cho ↑ , Ins ↑ , NAA/tCr ↓
Lim et al. (1997) (33)	10 (10/0)	20-28, 65-75	Centrum semiovale	1.5	MRSI	R	NAA (gm)/NAA (wm) ↓
Fukuzako et al. (1997) (22)	36 (17/19)	24.7-78.6	Left medial temp.	2	MRS	R	NAA/tCR ↓
Pfefferbaum et al. (1999) (29)	34 (24/10)	25.3 ± 2.9, 73.3 ± 4.1	Centrum semiovale	1.5	MRSI	A (i.u.)	tCr ↑ , Cho ↑
Saunders et al. (1999) (30)	30 (17/13)	24-89	Par. WM, occ GM	1.5	MRS	A (IWR)[e]	tCr ↑
Lundbom et al. (1999) (16)	12 (0/12)	35 ± 6, 74 ± 7	Frontal, par. And temp. WM and GM	1.5	MRSI	R	NAA/Cho ↓ , NAA/tCr ↓
Leary et al. (2000) (31)	44 (22/22)	22-62	Par. WM	1.5	MRS	A	tCr ↑ , Cho ↑
Angelie et al. (2001) (17)	32 (14/18)	21-61	Cortical GM, centrum semiovale, temp. (HC)	1.5	MRSI	R	S(NAA) ↓ , S(Cho) ↑ , S(tCr) ↑ , NAA/tCr ↓ , NAA/Cho ↓
Brooks et al. (2001) (18)	50 (50/0)	20-70	Frontal	1.5	MRS	A (EWR)[e,f] + R	NAA ↓ , NAA/tCr ↓
Grachev and Apkarian (2001) (25)	35 (23/12)	19-31, 40-52	Cingulate, thalams, insula, DPFC, OFC, SMC	1.5	MRS	R	NAA/tCR ↓ , Glu/tCr ↓ , Gln/tCr ↓ , Glc/tCr ↓ , Lac/tCr ↓ , GABA/tCr ↓
Harada et al. (2001) (26)	50	20-70	Frontal, lentiform n.	1.5	MRS	A (IWR)[e]	NAA ↓
Kadota et al. (2001) (19)	90 (45/45)	4-88	Centrum semiovale	1.5	MRSI	R	NAA/Cho ↓
Schuff et al. (2001) (27)	40 (18/22)	56-89	Frontal and par.	1.5	MRSI	A (a.u.)[e]	NAA ↑ , tCr ↑
Driscoll et al. (2003) (34)	32 (16/16)	20-39, 60-85	HC, frontal WM	1.5	MRS/I	R	NAA/tCr ↓
Szentkuti et al. (35)	35 (16/19)	22-27, 60-75	HC, extraHC	1.5	MRS	R	NAA/(tCr+Cho) ↓
Charlton et al. (2007) (28)	106 (55/56)	50-90	Centrum semiovale	1.5	MRSI	A	NAA ↑ , tCr ↑
Sailasuta et al. (2008), (20)	50	21-71	Frontal GM/WM, par. GM, basal ganglia	3	MRSI	A (i.u.)[e]	NAA ↓ , Glu ↓
Chang et al.(2009)[b] (23)	63 (24/39)				MRS/I		NAA ↓ , tCr ↑ , Cho ↑ , Ins ↑ , NAA/Cho ↓ , NAA/tCr ↓ , Cho/tCr ↑ , Ins/tCr ↑
Gruber et al. (2009) (21)	63 (24/39)	18-65	Emp., DPFC (WM), frontal and par., thalamus, caudate n., lentiform n.	3		A (IWR)[f] + R	
Raininko and Mattson (2010) (24)	57 (32/25)	13-72	Supraventricular WM	1.5	MRS	A (IWR)	NAA ↓ , Ins ↑

Table 2 Literature survey of ^{1}H-MRS studies in normal aging. [a] Size refers to the number of subjects in the study; M/F = male/female ratio. [b] This study is a revision of Sailasuta et al. (2008). [c] WM = white matter; GM = gray matter; temp. = temporal; par. = parietal; occ. = occipital; HC = hippocampus; DPFC = dorsolateral prefontal cortex; OFC = orbitofrontal cortex; SMC = sensorimotor cortex; extraHC = extrahippocampal; n. = nucleus. [d] A = absolute; R = relative; EWR = external water reference; IWR = internal water reference; i.u. = institutional units; a.u. = arbitrary units. [e] Corrected for CSF. [f] Corrected for T_1 and T_2; [g] results were included at a significance level $P<0.05$, unless mentioned otherwise.

Mild Cognitive Impairment (MCI)

Mild cognitive impairment (MCI) has been described as a transitional state between the cognitive changes following normal aging and those of very early dementia. It is a prodromal phase of a range of potential conditions such as, frontotemporal dementia, dementia with Lewy bodies, vascular dementia and most frequently Alzheimer's disease. In 1999 the first criteria for the diagnosis of MCI were set, consisting of the following: memory complaints, preferably corroborated by an informant; memory impairment documented according to appropriate reference values; essentially normal performance in non-memory cognitive domains; generally preserved activities of daily living (ADL); not demented state. (36) Prevalence seems to converge globally between 14% and 18% for individuals aged 70 years and older. (37)

Diagnosing and categorizing MCI

Further research revealed that not all MCI subjects suffer from solely amnestic cognitive difficulties or evolve to Alzheimer's disease. In 2003, the diagnostic criteria were revised to include other forms of cognitive impairment. (38) These domains encompass language, attention, executive functions, visuospatial skills, problem-solving skills, constructional praxis and behavioral features. This revision essentially led to two main subtypes: amnestic MCI (with mainly memory impairment) and non-amnestic MCI (with non-memory cognitive impairment). This classification was expanded to create a diagnostic algorithm that allows for subtyping MCI patients. (see fig. 13)

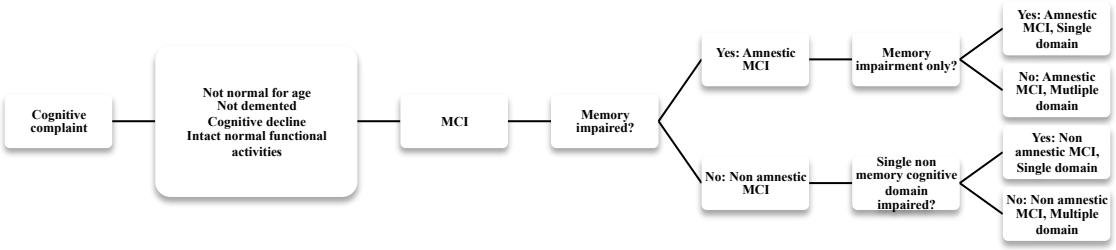

Figure 13 Diagnostic Algorithm for diagnosing and categorizing MCI. (37)

The diagnostic process starts after an official complaint is made about the person's cognitive function, often by an informant. Next, the clinician will take the patient's history and perform a mental status exam (e.g. a mini mental state exam, MMSE). With these results the patient is categorized as either normal or demented. For example, an MMSE score of 20 out of 30 with

functional impairment may lead to the diagnosis of dementia, whereas a score of 29 out of 30 without functional impairment is considered as normal, regardless of the original complaint. Of course, other diagnoses have to be checked such as, depression, delirium, etc. In some cases uncertainty concerning the cognitive status may arise and the diagnosis of MCI is retained. When the patient is regarded as neither normal nor demented, further investigations are needed. Memory and other cognitive domains are assessed by means of neuropsychological testing, e.g. using the Clinical Dementia Rating Scale (CDR). (40) Further classification can be made by means of the diagnostic scheme of Petersen et al. (37) (see fig. 13) In light of a prognostic outcome, an investigation is started to determine potential pathogenesis. By means of history taking, laboratory testing and neuroimaging, the clinician determines a likely cause of the cognitive impairment: degenerative (gradual onset, insidious progression), vascular (abrupt onset, vascular risk factors, history of cardiovascular diseases), psychiatric (depression or anxiety) or a concomitant medical disorder (heart failure, diabetes, cancer). (39)

Conversion from MCI to dementia

Aging in itself is a variable process and so is the progression from MCI to dementia. Studies have demonstrated yearly conversion rates from 6% up to 15% in MCI patients (36, 41, 42, 43), which far exceeds the general population incidence of 1-2% a year. (37) In MCI this conversion is influenced by several factors that can be regarded as predictors for rapid progression: the severity of cognitive impairment; genetic predisposition (positive apolipoprotein E ε4 carrier status); neuroimaging status (general cerebral atrophy, reduced hippocampal volume, reduced entorhinal cortex volume, increased ventricular volume, medial temporal and left parietal gray matter volume (37, 44) hypometabolism in the temporoparietal regions as determined by Fluodeoxy F18-positron emission tomography (^{18}FDG PET)); biomarkers in cerebrospinal fluid (CSF) such as low amyloid β 1 to 42 peptide ($A\beta_{1-42}$), high total tau protein, and high tau phosphorylated at threonine 181 (45); raised amyloid depositions on imaging; neurofibrillary tangle density. (37) It is most likely that a combination of these predictors will provide an informative prospect into the prognosis of a patient. (46)

Studies have shown a link between the likely etiology of MCI and the potential outcome. (see fig. 17, 39) Amnestic MCI subtypes with presumed degenerative etiology may convert to Alzheimer's disease. (38) Non-amnestic MCI subtypes are more likely to progress to non-Alzheimer's dementia. (47)

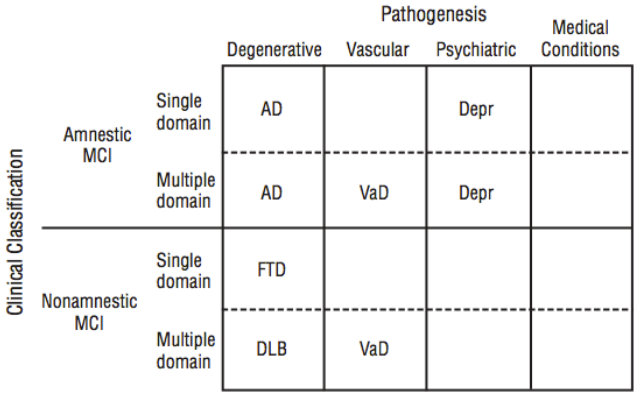

Figure 14 Predicted outcomes of MCI Subtypes according to Pathogenesis. (37) AD = Alzheimer's Disease; Depr = depression; DLB = dementia with Lewy Bodies; FTD = frontotemporal dementia; VaD = vascular dementia.

Pathophysiology of MCI

For Alzheimer's disease the major neuropathological findings, i.e. neurofibrillary tangles (NFT) and senile plaques (SP) (also known as extracellular deposits of amyloid beta peptide), are well studied, but these results should not be blindly extrapolated to MCI. The Religious Order study (48) found cerebral infarctions, neurofibrillary pathology and Lewy bodies among MCI patients. Moreover, NFT increases in amygdala, entorhinal cortex, CA1 (Cornu Ammonis, hippocampus), subiculum and inferior parietal lobule were significantly correlated with episodic memory loss. In another study a broad spectrum of pathological findings were seen: hippocampal sclerosis, infarctions, Lewy bodies and argyrophilic granulation. (39) It appears that neurofibrillary pathology in medial temporal lobe structures is the major determinant for MCI and memory regression, not amyloid plaques. (49)

^{1}H-MRS in MCI

^{1}H magnetic resonance spectroscopy has also been used to study metabolic changes in MCI patients. Table 3 shows recent results, depicting a clear image of metabolic differences between MCI patients and age-matched controls. Only significant (P<0.05) results were included, some trends are indicated with specific P value. NAA/tCr was often lower in MCI groups than in controls in the posterior cingulate cortex (PCC) (50, 51, 52, 53). Decreased absolute NAA concentrations (51), elevated levels of mI/Cr (53, 54) and increases in mI/NAA (53) were also found in the PCC.

In the left parietal and frontal cortex both NAA/tCr and absolute NAA concentrations were decreased (55).

NAA/H_2O ratio was decreased in the medial temporal lobe and parietotemporal cortex (56).

^{1}H-MRS in the hippocampus provided little significant differences in general, compared to controls, except for decreased Glu/mI (57), elevated mI/Cr (58) and decreased tCr (59).

In conclusion, MCI patients are of diverse etiology and represent a stage of impairment beyond what is normal for age, but not of sufficient magnitude as to warrant the diagnosis of dementia or Alzheimer's disease. (39) Research about MCI has exploded during the last two decades, searching for clinical insights and working towards early diagnosis and treatment of cognitive decline.

Study	**Size** (MCI/Controls)[a]	**Age range**	**Regions of interest**[b]	**B** (T)	**Quantification**[c]	**Results**[d]
Chantal et al., 2004 (56)	28 (14/14)	69.2 ± 6.8; 71.1 ± 7.5	MTL, PTC, PFC	1.5	R, IWR	NAA/H2O ↓ ; Cho/H2O ↓
Kantarci et al., 2006 (52)	137(49/88)	78.0 ± 8.5; 79.1 ± 7.2	posterior cingulate cortex & precuneus	1.5	R	NAA/Cr ↓ ; Cho/Cr ↓
Pilatus et al.,2007 (51)	27 (15/12)	70.0 ± 5.8; 64.4 ± 5.0	posterior cingulate cortex, PVPWM	1.5	A, EWR[e, f]	NAA ↓ ; NAA/tCr ↓
Garcia Santos et al., 2008 (60)	44 (10/34)	73.5 ± 7.0; 72.9 ± 6.2	posterior cingulate cortex & precuneus	1.5	R	-
Kantarci et al., 2008 (54)	243 (143/100)	76 ± 5; 78 ± 6	posterior cingulate cortex & precuneus	1.5	R	mI/Cr ↑
Kantarci et al., 2009 (52)	151	50-93	posterior cingulate cortex & precuneus	1.5	R	NAA/Cr ↓ (P =0.06)
Zhang et al., 2009 (58)	27 (14/13)	74.1 ± 4.8; 72.2 ± 8.5	left hippocampus,temporopar. White matter	1.5	R	mI/Cr ↑
Jessen et al., 2009 (61)	181 (136/45)	66.5 ± 8.4; 65.4 ± 7.8	hippocampus	1.5	R + A, IWR[e, f]	-
Wang et al., 2009 (53)	32 (16/16)	72.1 ± 8.0; 71.1 ± 11.1	posterior cingulate cortex	3	R	mI/Cr ↑ ; mI/NAA ↑ ; NAA/Cr ↓
Li et al., 2010 (55)	68 (34/34)	72.5 ± 5.4; 71.6 ± 5.7	left frontal, left par., right par. Cortex	1.5	R + A (a.u.)	NAA ↓ ; NAA/Cr ↓ (L temp./par.)
Rupsingh et al., 2011 (57)	27 (12/15)	71.8 ± 9.9; 78.3 ± 5.9	hippocampus	4	R + A, IWR[e, f]	mI ↑ (P < 0.1); Glu/NAA ↓ (P<0.1); Glu/mI ↓
Foy et al., 2011 (59)	60 (21/39)	mean 76	hippocampus	1.5	A, IWR[e, f]	tCr ↓

Table 3 Literature Survey of ^{1}H-MRS studies in normal aging. [a] Size refers to the number of subjects in the study; [b]par. = parietal; occ. = occipital; PVPWM periventricular parietal white matter; MTL = medial temporal lobe; PFC = prefrontal cortex, PTC = parietotemporal cortex; [c]A = absolute; R = relative; EWR = external water reference; IWR = internal water reference; i.u. = institutional units; a.u. = arbitrary units; [d] results were included at a significance level P<0.05, unless mentioned otherwise; [e]Corrected for CSF; [f]Corrected for T_1 and T_2.

Materials and Methods

Subjects

NOMARED

90 healthy subjects took part in a ^{1}H-MRS study, called NOMARED (Normal age-related Magnetic REsonance Database). The subjects for this study were recruited through advertisements in the hospital. Demographics are summarized in table 4.

Age	Total Subjects	Females	Males	PCC[a]	HC[a]
<30	20	13	7	19	16
31-40	12	4	8	10	11
41-50	11	6	5	10	10
51-60	17	8	9	16	14
61-70	22	7	15	20	21
>70	8	4	4	8	7
Total	90	42	48	83	79

Table 4 Demographic summary of healthy volunteers studied in the different brain regions. [a]Values reflect the number of spectra included in the analysis.

All subjects underwent a clinical medical and neurological examination (by a neurologist) and a structured psychiatric interview (by a psychiatrist) to exclude (a history of) neurological and psychiatric disorders. Exclusion criteria were based on history including disorders of the central nervous system, such as (possible) epilepsy, head trauma, cerebrovascular accidents, migraine, neurodegenerative disease, as well as psychiatric disorders such as substance abuse or mood and anxiety disorders.

To exclude cognitive impairment, volunteers underwent thorough neuropsychological testing including the following standardized tests: the Dutch version of the Auditory Verbal Learning Test (AVLT) (62), the Visual Association Test (VAT), the Trail Making Test Parts A and B, the COntrolled Word Association Test (COWAT), the Stroop Color Word Test, the Digit Span Test, the Purdue Pegboard Test and the Standardized Money Road Map Test. Handedness was investigated by the Briggs and Nebes questionnaire.

Medication, such as contraceptives in young women, hormonal replacement therapy in postmenopausal women, antihypertensive and cholesterol lowering medication in the elderly were allowed, except for the use of current and past (3 months) psychoactive drugs (e.g., anxiolytic, antidepressant, antiepileptic drugs). Subjects with medical conditions such as hypertension, hypercholesterolemia or diabetes mellitus type II treated and under control by oral medication were not a priori excluded.

For inclusion in the study, test results on the AVLT and VAT that specifically interrogate

temporal lobe function, had to be within the normal range (results matched for age, gender and education). The local ethics committee approved the study and all subjects gave written informed consent.

In 31 subjects the MRI showed small to larger periventricular and deep white matter lesions. These lesions were not localized in both examined brain regions and in most cases these lesions were attributable to normal age-related changes, and hence, were not excluded from the study. In 8 to 12 % of the cases, the MR data could not be evaluated due to suboptimal quality of the images and/or spectra, caused by bad shimming or motion artifacts. (see table 4)

MCI

6 healthy controls and 8 Mild Cognitive Impaired (MCI) patients were thusfar included in the ongoing MCI study. In this study patients are compared to control subjects as to unravel parts of the pathophysiology of pathological aging. All patients underwent a clinical medical and neurological examination (by a neurologist) and a structured psychiatric interview, including a Mini Mental Status Exam (MMSE), Cinical Dementia Rating (CDR) and a auditory-verbal learning test (aVLT) to confirm the MCI diagnosis. Main exclusion criteria were non-MR compatible implants. Control subjects were mainly informants of the patients, who were involved in the diagnostic path of the patient. The local ethics committee approved the study and all subjects gave written informed consent. Demographics are a shown in table 5.

	controls	**MCI**	**total**
total subjects	6	8	14
female	4	6	10
male	2	2	4
age (mean ± SD)	62.7 ± 11.7	69.1 ± 12.9	66.3 ± 12.4

Table 5 Demographic summary of MCI patients and control subjects.

NOMAREDplus

Upon processing the NOMARED data , it was decided to extend the NOMARED study with 10 young adults, in order to perform measurements to include T_1 and T_2 corrections. Male to female ratio was 1:9, subject mean age was 22.9 ± 1.6 years. All subjects gave written informed consent.

MRS

NOMARED

Within the NOMARED study all subjects had to participate in both a PET- and a multimodal MR-study, including structural MRI, MRS, ASL and resting-state fMRI. This thesis covers only the MRS-data. All measurements were performed on a 3 T Siemens TrioTim whole-

body scanner (Erlangen, Germany), using a standard Siemens birdcage 8-channel head coil. Structural images were acquired with a T_1-weighted gradient-echo image (MPRAGE) in three orthogonal planes with a slice thickness of 1 mm, a *TR* of 1550 ms and a *TE* of 2.37 ms, a 256 x 256 matrix and 176 slices. Spectra were acquired using a STEAM pulse sequence in the left HC and a PRESS pulse sequence in the PCC. (see fig. 15) The voxel size was 25 x 20 x 12 mm^3 and 20 x 20 x 20 mm^3 in the HC and the PCC, respectively. For STEAM, magnetic resonance parameters were: *TR* 1500 msec, *TE* 20 msec and 144 msec, *TM* 10 msec, 128 measurements, dwell time per point 833 msec for 1024 data points, and corresponding bandwidth 1200 Hz. For PRESS, MR parameters were: *TR* 1500 msec, *TE* 30 msec, 128 measurements, dwell time per point 833 msec for 1024 data points, and corresponding bandwidth 1200 Hz. Automatic shimming with manual fine tuning of the B_0 magnetic field and semi-automated optimization of the transmitter voltage were used. Weak water suppression was used in order to use the residual water signal as an internal reference for relative quantification. In the PCC of 57 subjects, the cerebrospinal fluid (CSF) content was measured in the same voxel according to the method of Ernst et al., 1993. (69) We measured the unsuppressed water signal with a PRESS sequence with 10 different echo times (30, 50, 70, 90, 110, 150, 200, 300, 500 and 1000 msec) in the PCC of 57 subjects.

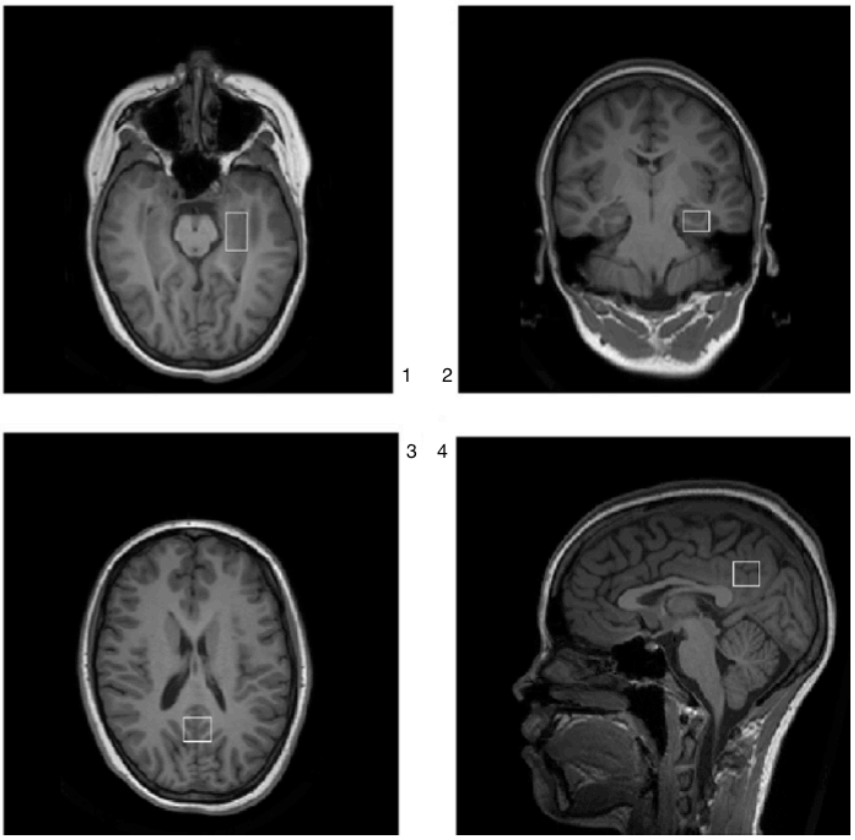

Figure 15 T_1 weighted images illustrating voxel placement: [1] axial localization of HC; [2] coronal localization of HC; [3] axial localization of PCC; [4] sagittal localization of PCC.

MCI

For the MCI study subjects a similar PRESS sequence was used for both posterior cingulate cortex and hippocampus measurements, MR parameters were: *TR* 1500 msec, *TE* 30 msec, 128 measurements, dwell time per point 833 msec for 1024 data points, and corresponding bandwidth 1200 Hz. The CSF content was determined as described in the NOMARED study in both PCC and HC.

NOMAREDplus

In subjects of the NOMAREDplus study we tried to determine T_1 and T_2 relaxation times (used in absolute quantification, see below) experimentally. In the first 5 subjects following spectra were acquired: firstly spectra in both PCC and HC, with *TR* 1500 msec, *TE* 30 msec, 128 measurements, dwell time per point 833 msec for 1024 data points, and corresponding bandwidth 1200 Hz; and secondly, for the determination of T_2, water-suppressed PRESS sequences with six different echo times (*TE*= 30, 60, 90, 120, 144 and 288ms), a *TR* of 4000ms and 64 averages, were performed in both PCC and HC. In the final 5 subjects following spectra were acquired: firstly in both PCC and HC, a PRESS sequence with *TR* 1500 msec, *TE* 30 msec, 128 measurements, dwell time per point 833 msec for 1024 data points, and corresponding bandwidth 1200 Hz; and secondly, the same water-suppressed PRESS sequence was used with eight different repetition times (*TR* = 1500, 2000, 2500, 3000, 3500, 4000, 6000 and 10000 ms), a *TE* of 30 ms and 64 averages, in order to determine T_1 relaxation times. Due to time restrictions the latter spectra were only acquired in the PCC. In all 10 subjects CSF content was determined in both PCC and HC.

Quantification

Signal processing

Before quantification of the metabolite ratios and/or absolute metabolite concentrations, the signal (peak) areas need to be determined. This step is often laborious, caused by a number of reasons: a strong overlap in metabolic peaks (large number), a low signal-to-noise ratio (SNR) and a broad background signal due to macromolecules and lipids that overlap metabolic peaks. (63)

In NOMARED and MCI studies signal areas were assessed using the scanner software, syngoMR B15, Numaris 4. Before determination of the signal, a number of preprocessing steps were required including apodization (Hanning filter, width 400 ms), zero-filling to 2048 points, and the Fourier transformed FIDs (polynomial 8^{th} order) were baseline and phase corrected. The signals of NAA, tCr, Cho, Ins and H_2O, at reference points 2.01, 3.03, 3.19, 3.52 and 4.70 ppm, repectively, were quantified by measuring peak areas. These were obtained by a Levenberg-Marquardt algorithm using the scanner software. (64)

In the NOMAREDplus study signal areas were determined, using both the scanner software as well as two algorithms included in the jMRUI software package, QUEST and AMARES. (65) AMARES (Advanced Method for Accurate, Robust and Efficient Spectral fitting) is a sophisticated non-linear, least squares algorithm for quantitation. The main advantages of AMARES include the more extended input of prior knowledge, the use of Gaussian instead of Lorentzian line shapes for peak and background signals and the possibility of applying soft constraints (i.e. imposing lower and upper bounds) on the freely estimated parameters. (66, 67) QUEST (quantitation based on QUantum ESTimation) relies on extensive prior knowledge input, based on quantum mechanical properties of in vitro metabolic solutions.

Water signals were processed with the Numaris 4 software, using the same algorithm, but without using the automated *water processing* function. These signals were also quantified with a black-box signal-processing algorithm in jMRUI, the Hankel Lanczos singular value decomposition algorithm (HLSVD) (68).

Quantification

Analysis of the data was done by means of relative quantification (ratios of NAA/tCr, Cho/tCr, Ins/tCr, NAA/H_2O, tCr/H_2O, Cho/H_2O and Ins/H_2O) and absolute quantification. Absolute quantification was based on the internal water reference and was performed in the PCC of 57 subjects in the NOMARED study. To perform absolute quantification, a number of correction factors need to be determined, as depicted in equation 1.

$$c_{met} = \frac{S_{met} \cdot k_{met}}{S_{H_2O} \cdot k_{H_2O}} \cdot \frac{N_{H_2O}}{N_{met}} \cdot \frac{1}{1 - f_{CSF}} \cdot c_{H_2O}$$

Equation 1

C_{met} represents the metabolite concentration; S_{met} and S_{H2O} are the signal intensities; k_{met} and k_{H2O} are correction factors for T_1 and T_2 relaxation of the specific metabolite and of water; N_{met} and N_{H2O} represent the number of hydrogen atoms in the spectrum peak (N for H_2O =2, for NAA N =3, for Cho N =9); f_{CSF} is the fraction of CSF in the voxel; c_{H20} is the internal water reference concentration.

CSF fraction

For determining the CSF fraction and k_{H2O}, the unsuppressed water signal was acquired as described earlier in the PCC of 57 subjects. The signal intensity (S) of the unsuppressed water signal was plotted against *TE* using MATLAB software (Mathworks, Natick, MA). The signal amplitudes of CSF and brain water were extracted using a Levenberg-Marquardt algorithm (equation 2), according to the method of Ernst et al., 1993. (69)

$$S = S_{CSF} e^{\frac{-TE}{T_{2,H_2O,CSF}}} \cdot (1 - e^{\frac{-TR}{T_{1,H_2O,CSF}}}) + S_{BW} e^{\frac{-TE}{T_{2,H_2O,BW}}} \cdot (1 - e^{\frac{-TR}{T_{1,H_2O,BW}}})$$

Equation 2

S represents the signal intensity of the unsuppressed water. Using this equation, following parameters could be extracted: $T_{1,H2O,CSF}$, $T_{2,H20,CSF}$, $T_{1,H2O,BW}$ and $T_{2,H20,BW}$ are the relaxation times of CSF and brain water (BW); S_{CSF} and S_{BW} are the unrelaxed signal amplitudes of CSF and brain water. CSF values corresponded to signal intensities with longer T_2.

The fraction of CSF (f_{CSF}) is determined by equation 3.

$$f_{CSF} = \frac{S_{CSF}}{S_{CSF} + S_{BW}}$$

Equation 3

The correction factor for water (k_{H2O}) was determined using equation 4, using results from equations 2 and 3. The fraction of brain water (f_{BW}) equals (1-f_{CSF}).

$$k_{H_2O} = \frac{f_{BW}}{(1 - e^{\frac{-TR}{T_{1,H_2O,BW}}}) \cdot e^{\frac{-TE}{T_{2,H_2O,BW}}}} + \frac{f_{CSF}}{(1 - e^{\frac{-TR}{T_{1,H_2O,CSF}}}) \cdot e^{\frac{-TE}{T_{2,H_2O,CSF}}}}$$

Equation 4

T_1 and T_2 relaxation times

The correction factor for the metabolite (k_{met}) was determined using equation 5, where $T_{1,met}$ and $T_{2,met}$, the relaxation times of the metabolite, were obtained from literature. (70)

$$k_{met} = \frac{1}{(1 - e^{\frac{-TR}{T_{1,met}}}) \cdot e^{\frac{-TE}{T_{2,met}}}}$$

Equation 5

$T_{1,met}$ and $T_{2,met}$ that are used in equation 5, can also be determined experimentally. As mentioned, acquired signals must be corrected for T_1 and T_2 decay as the measurement was performed with a *TE* of 30 ms and a *TR* of 1500 ms, corresponding with a considerable loss of signal in the transverse plane and a not fully relaxed signal in the longitudinal direction, respectively. In NOMAREDplus, the determination of T_2 was performed with the same water-suppressed PRESS sequence with six different echo times (*TE*= 30, 60, 90, 120, 144 and 288ms), a *TR* of 4000ms and 64 averages. The same water- suppressed PRESS sequence was used with eight different repetition times (*TR* = 1500, 2000, 2500, 3000, 3500, 4000, 6000 and 10000 ms), a *TE* of 30 ms and 64 averages. T_1 and T_2 relaxation times were calculated by fitting the peak areas determined by Numaris 4, to single-exponential functions, using a Levenberg-Marquardt algorithm in MATLAB (Mathworks, Natick, MA), in which the signal was plotted against *TE* or *TR*, respectively, using equations 6 and 7. (70)

$$S = S_0(1 - e^{\frac{-TR}{T_1,met}}) \qquad S = S_0 e^{\frac{-TE}{T_{2,met}}}$$

Equation 6 **Equation 7**

Water concentration

The concentration of H_2O in the voxel, c_{H2O}, can be determined using equation 8, where $c_{H20,BW}$ and $c_{H20,CSF}$ are the concentrations of water in brain tissue and CSF. In literature, the water concentrations are 52.3 M and 45.8 M in gray and white matter, respectively, and 55.5 M in CSF. (71) Because segmentation was not performed, an average water concentration of 49 M was used for the brain water fraction, as combined white and gray matter fraction.

$$c_{H_2O} = f_{BW} \cdot c_{H_2O,BW} + f_{CSF} \cdot c_{H_2O,CSF}$$

Equation 8

Flowchart

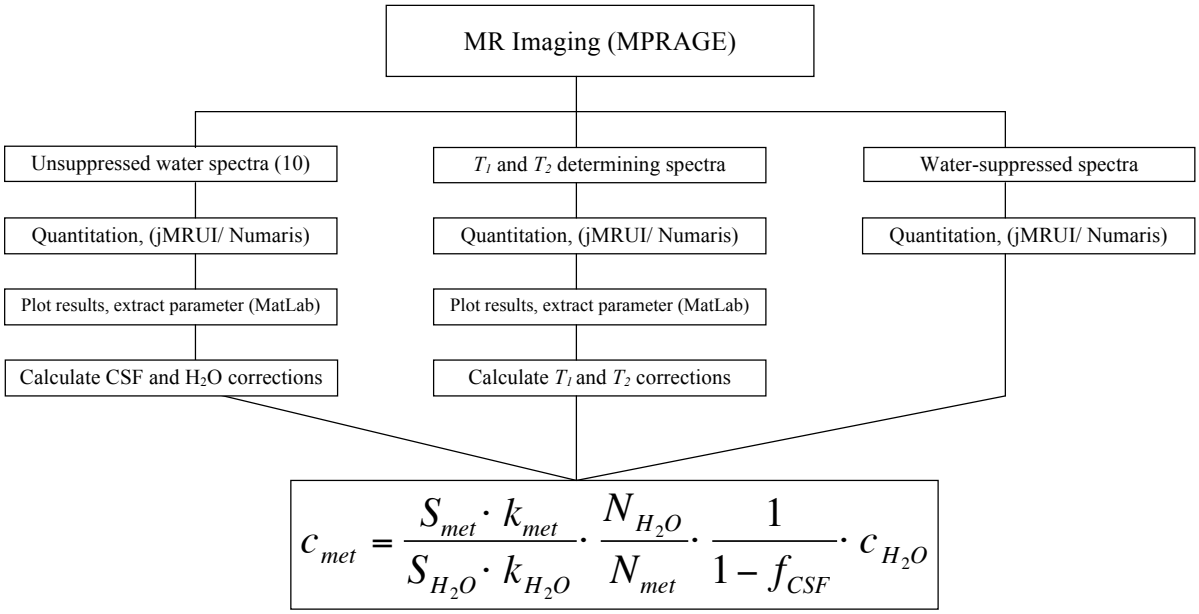

Figure 16 Flowchart in quantification of brain metabolites.

Statistical analysis

Statistical analysis was performed using SPSS software (SPSS 19.0 for Windows; Chicago, IL). Descriptive statistics were applied for age, metabolite ratios and absolute metabolite concentrations in the NOMARED study. An unpaired Student's t-test was applied to compare CSF fractions, metabolite ratios and absolute concentrations between males and females. Analysis of covariance (ANCOVA) was performed, with age as covariate, in order to determine the interaction effect between age and gender on metabolite ratios and absolute concentrations. Linear regression analysis was performed to investigate the association between age and CSF fraction, metabolite concentrations or absolute concentrations. Pearson correlation matrix analysis was used to scout for correlations between metabolite ratios and absolute concentrations.

In the MCI study an unpaired Student's t-test was applied to compare CSF fractions, metabolite ratios and absolute concentrations between control subjects and MCI patients. Analysis of covariance (ANCOVA) was performed, with age as covariate, in order to determine the interaction effect between age and study group on metabolite ratios and absolute concentrations. Linear regression analysis was performed to investigate the association between age and CSF fraction, metabolite concentrations or absolute concentrations.

In NOMAREDplus study descriptive statistics were used for CSF fractions. Linear as well as quadratic regression was applied in order to investigate the association between age and CSF fraction.

Results

NOMARED

Age differences

Tables 6 and 7 show results of the ANCOVA analysis of metabolic ratios and absolute concentrations, in the researched brain areas, including *P*-values for age, gender and gender-by-age effects. Graphical dot plots of statistical findings in the PCC are shown in figures 17 - 24, each depicted with a trend line.

In the PCC, a significant age-related Ins increase was found in Ins/tCr, Ins/H_2O and [Ins] (P<0.05). (see fig. 19, 20 and 23, respectively) In the HC, an age-related significant increase was also observed for Ins/tCr and Ins/H_20 (P<0,01). We found a significant positive correlation in the PCC between [Ins] and age (P<0.001, R=0.43). (see fig. 23) A significant age-dependent raise in tCr/H_2O was seen in the PCC (P=0.002). (see fig 17) A significant positive correlation was found between [tCr] and age (P<0.001, R=0.62) in the PCC. (see fig. 22)

Furthermore, Cho/tCr was significantly decreased with age (P=0.019) in the PCC (see fig. 18), in contrast to non-significant Cho/H_2O or [Cho] changes.

In the PCC, borderline significant age-related changes were found for NAA/tCr and [NAA] (respectively, P=0.097 and P=0.072). (see fig. 21)

The CSF fraction increased significantly with age (P<0.001). Mean CSF content in studied voxels in the PCC was 7.3 ± 3.5%. There was a significant linear correlation between age and CSF content (P<0.001, R=0.63). (see fig. 24)

	PCC			HC		
	Age	**Gender**	**Age x gender**	**Age**	**Gender**	**Age x gender**
NAA/tCr	0.097	0.207	0.361	0.158	0.219	0.345
Cho/tCr	**0.019**	0.935	0.916	0.918	0.620	0.684
Ins/tCr	**0.035**	0.352	0.203	**0.003**	0.849	0.217
NAA/H_2O	0.313	**0.009**	**0.029**	0.063	0.123	0.191
tCr/H_2O	**0.002**	0.113	0.143	0.915	0.932	0.857
Cho/H_2O	0.582	0.325	0.378	0.707	0.530	0.565
Ins/H_2O	**0.001**	0.952	0.663	**0.007**	0.745	0.199

Table 6 P-values of ANCOVA analysis of metabolite ratios vs age and gender in PCC and left HC. Significance levels with P <0.05 are shown in bold font.

	Concentrations (mM)	P values		
		Age	Gender	Age x gender
[NAA]	15.17 ± 1.59	0.072	0.196	0.162
[tCr]	9.32 ± 0.92	**< 0.001**	0.504	0.551
[Cho]	1.87 ± 0.36	0.682	0.365	0.459
[Ins]	6.04 ± 1.29	**0.001**	0.411	0.231

Table 7 Absolute comecentrations in mM and P-values of ANCOVA analysis of absolute concentrations vs age and gender in PCC . Significance levels with P <0.05 are shown in bold font.

Gender differences

Gender differences were only significant for NAA/H_2O in the PCC (*P*=0.009), with males showing a somewhat higher concentration. There was also gender-by–age interaction for NAA/H_2O in the PCC, thus rendering the ANCOVA analysis non-valid. The correlation without this effect was not significant (*P*=0.106).

NAA/tCr and [NAA] did not prove to be gender related in the PCC during ANCOVA analysis, but when linear regression was performed separately for females and males, NAA/tCr proved to decrease with age in males only (*P*=0.043), whereas [NAA] increased significantly only in females (*P*=0.030). Similarly, Ins/tCr and Ins/H_2O increased with age in females (*P*<0.05).

CSF fraction did not differ between sexes (*P*=0.805).

Correlation between ratios and concentrations

A Pearson correlation analysis confirmed significant correlations between the two metabolite ratios mutually (metaboliteX/tCr and metaboliteX/H_2O) (*P*<0.001). This effect was also observed between metabolite ratios and absolute metabolite concentrations.

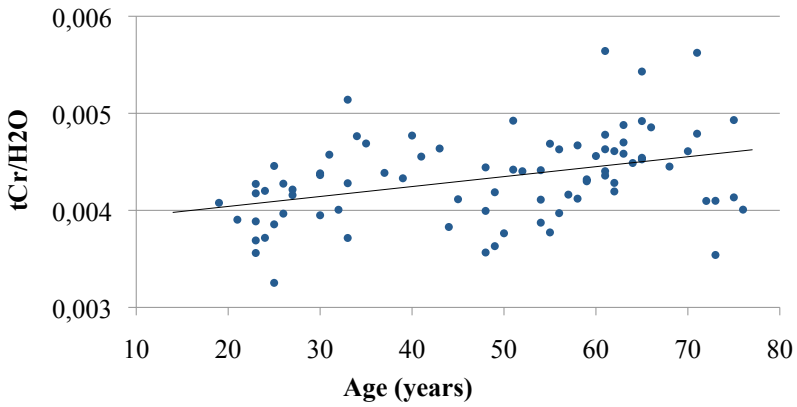

Figure 17 Linear regression plot of tCr/H_2O vs. age in the PCC. Trend equation: 'tCr/H2O = $1E^{-5}$ x age + 0.0038'; correlation coefficient R= 0.38.

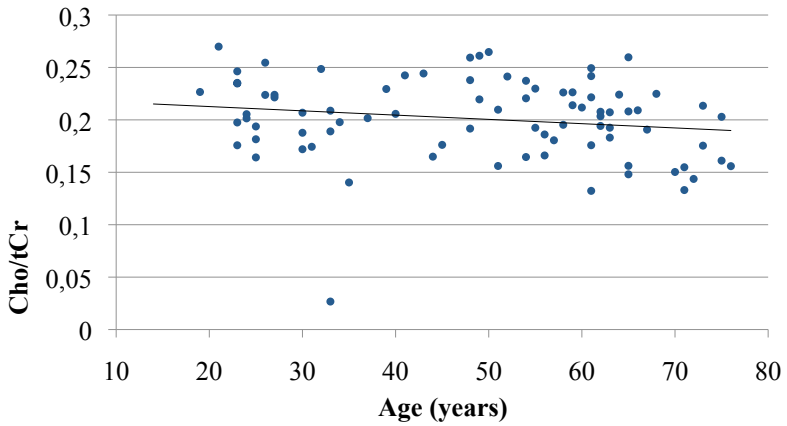

Figure 18 Linear regression plot of Cho/tCr vs. age in the PCC. Trend equation: 'Cho/tCr = -0.0004 x age + 0.2209'; correlation coefficient R= 0.22.

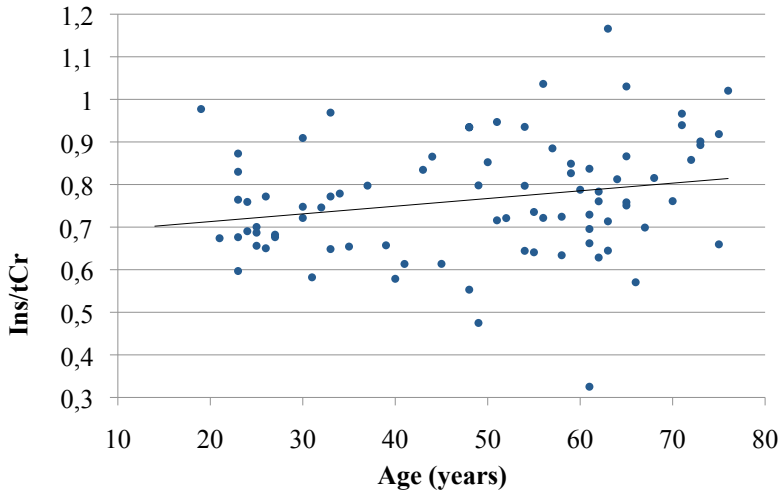

Figure 19 Linear regression plot of Ins/tCr vs. age in the PCC. Trend equation: 'Ins/tCr = 0.0018 x age + 0.6769'; correlation coefficient R= 0.23.

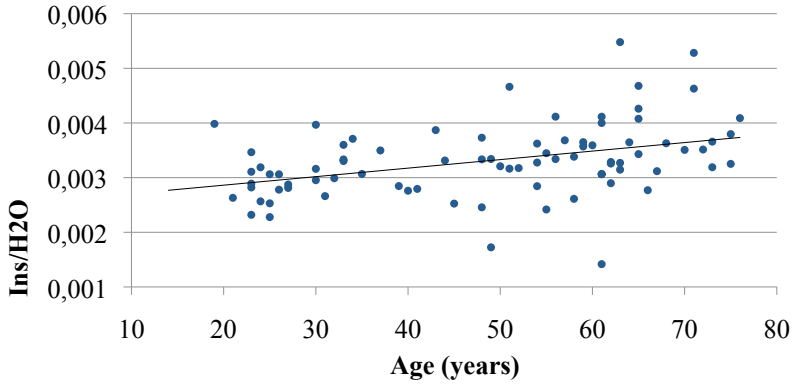

Figure 20 Linear regression plot of Ins/H_2O vs. age in the PCC. Trend equation: 'Ins/H2O = 2E^{-5} x age + 0.0026'; correlation coefficient R= 0.39.

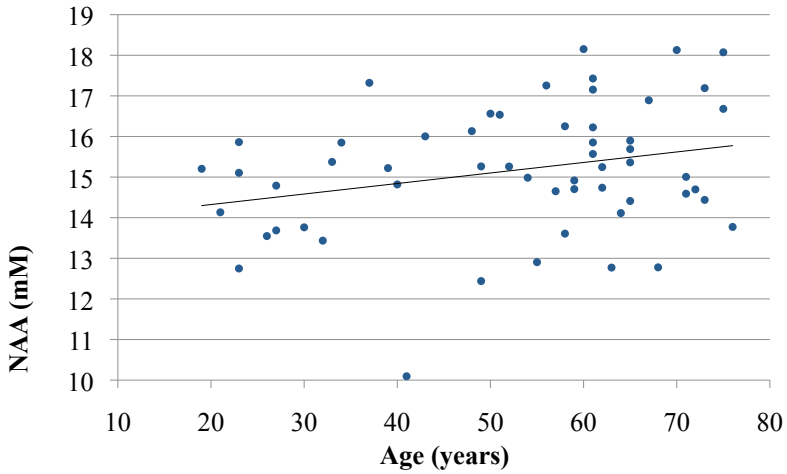

Figure 21 Linear regression plot of [NAA] vs. age in the PCC. Trend equation: '[NAA] = 0.0259 x age + 13.806'; correlation coefficient R= 0.27.

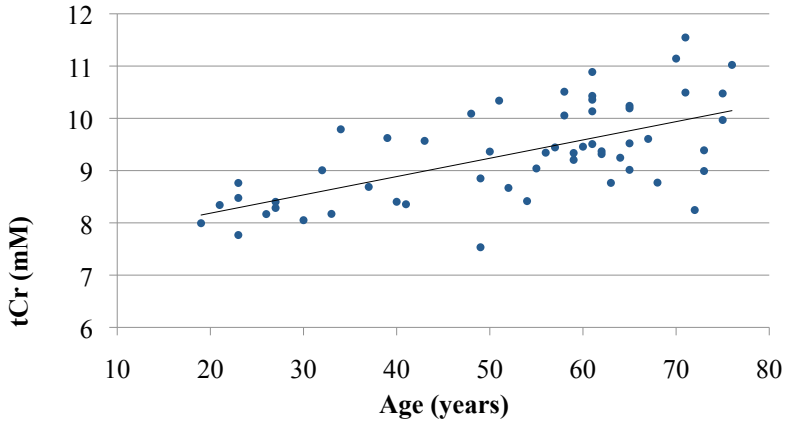

Figure 22 Linear regression plot of [tCr] vs. age in the PCC. Trend equation: '[tCr] = 0.035 x age + 7.484'; correlation coefficient R= 0.63.

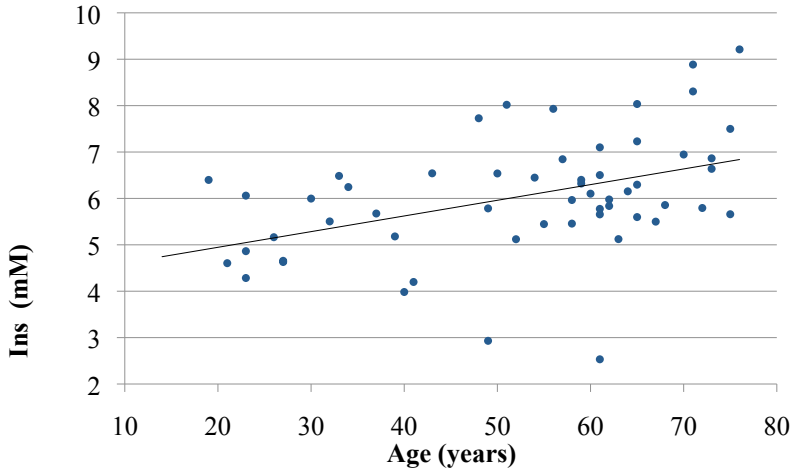

Figure 23 Linear regression plot of [Ins] vs. age in the PCC. Trend equation: '[Ins] = 0.0338 x age + 4,2708'; correlation coefficient R= 0.43.

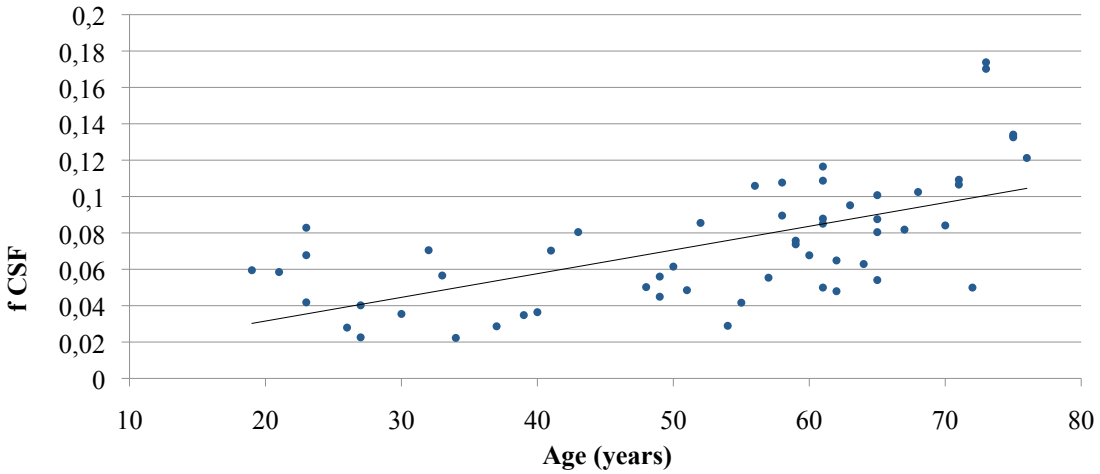

Figure 24 Linear regression plot of f_{CSF} vs. age in the PCC. Trend equation: 'f_{CSF} = 0.0013 x age + 0.0055'; correlation coefficient R= 0.63.

MCI

In the PCC spectra could be analyzed from 4 control subjects and 7 MCI patients. In the HC only 2 control subjects and 4 MCI patients could be assessed.

In the PCC, no metabolite ratio or absolute metabolite concentration was significantly correlated with age. (see table 8) Only CSF fraction was significantly increased with age in all subjects (*P*=0.012, *R*=0.72) (see fig. 25), in the control group (*P*=0.052), but not in the MCI group separately (*P*=0.167).

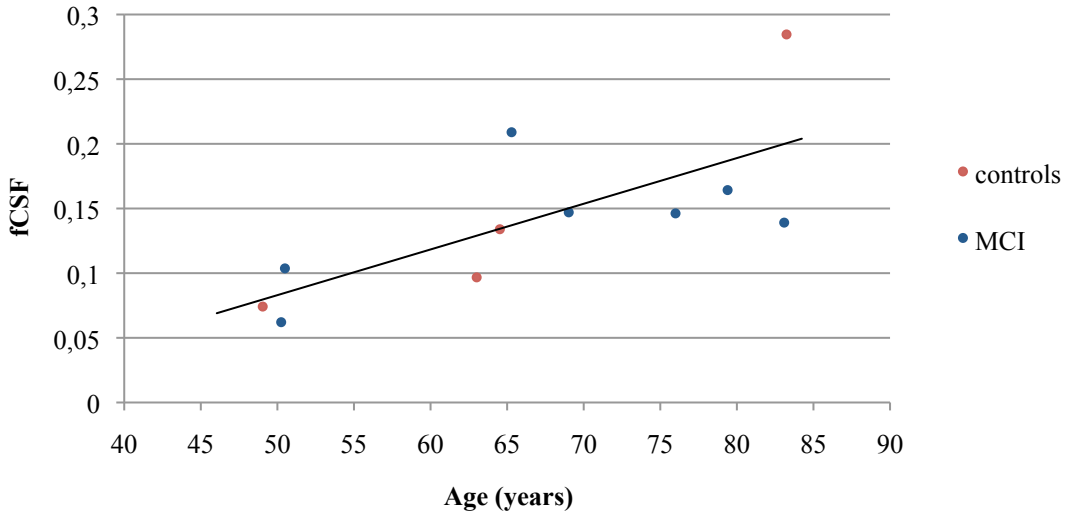

Figure 25 Linear regression plot of f_{CSF} vs. age in the PCC for MCI patients and control subjects together. Trend equation: 'f_{CSF} = 0.0035 x age – 0.0936'; correlation coefficient R= 0.72.

MCI patients and control subjects did not differ in any metabolite ratio or absolute metabolite concentration. A trend in increasing absolute Cho concentrations could be observed in the PCC (*P*=0.08). (see table 8) (see fig. 26)

Metabolite ratio or absolute concentration	***P* value**	
	t-test[a]	x age[b]
NAA/tCr	0.485	0.808
NAA/H_2O	0.442	0.240
Ins/tCr	0.111	0.686
Ins/H_2O	0.474	0.189
Ins/NAA	0.461	0.714
Cho/tCr	0.204	0.763
[NAA]	0.699	0.679
[tCr]	0.178	0.530
[Cho]	**0.082**	0.561
[Ins]	0.249	0.502
f_{CSF}	0.873	**0.012**

Table 8 Results from statistical analysis in MCI study in the PCC. [a] Means of MCI patients and control subjects were compared using independent sample t-test; [b] results from linear correlation with age, combining the results of MCI patients and control subjects. Significance levels with P<0.01 are shown in bold.

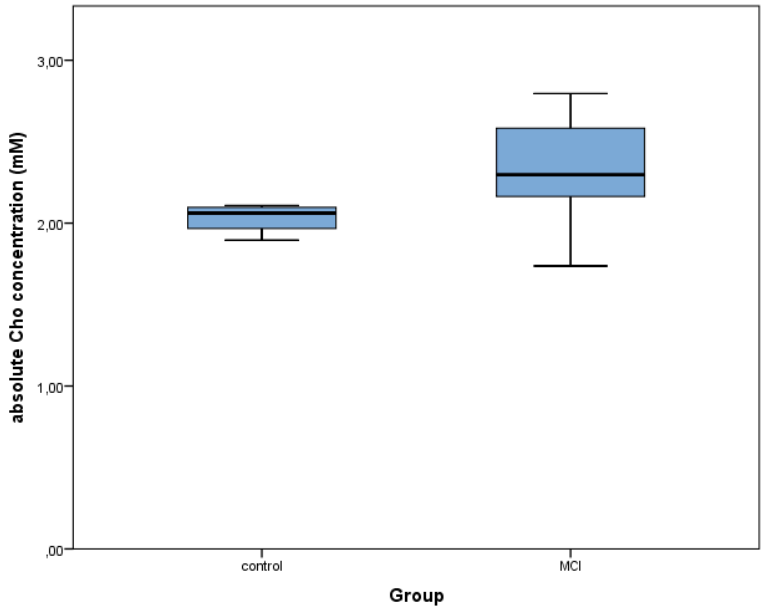

Figure 26 Box-and-whiskers plot comparing [Cho] between control subjects and MCI patients. Box-and whiskers plot depict from top to bottom: 97.5th percentile, 75th percentile, mean, 25th percentile and 2.5nd percentile. MCI patients showed an increase in [Cho] in the PCC compared to control subjects.

In the left HC no significant changes between control subjects and MCI patients could be observed.

NOMAREDplus

Experimental T_1 and T_2 relaxation times

T_1 and T_2 relaxation times for NAA, tCr, Cho, Ins and water in both CSF and brain fractions were experimentally determined and are shown in table 8. T_2 relaxation time for Cho could not be determined because of non-consistent results. The signal of Ins does not follow a single- or double-exponential with multiple echo times, and could therefore also not be determined.

Comparatively, results from literature are also shown in table 9. (70)

	Literature (70)		**Experimental**	
	T_1 (mean ± SD)	**T_2 (mean ± SD)**	**T_1 (mean ± SD)**	**T_2 (mean ± SD)**
H2O (CSF)	2897 ± 701	670 ± 120	2216 ± 1053	517 ± 278
H2O (BW)	484 ± 113	70 ± 6	343 ± 233	68 ± 7
NAA	1448 ± 99	224± 27	1596 ± 124	227 ± 61
tCr	1424 ± 146	146 ± 23	1585 ± 104	229 ± 67
Cho	1380 ± 232	148 ± 38	1371 ± 218	[b]
Ins	1113 ± 201	[a]	1087 ± 133	[a]

Table 9 Comparative table for T_1 and T_2 relaxation times for several metabolites and water. [a] The T_2-value of Ins could not be determined since the signal of Ins does not follow a single- or double-exponential with multiple echo times; [b] did not give consistent results.

CSF fractions

CSF fractions calculated for NOMAREDplus subjects were added to the results of the NOMARED study. The CSF fraction decreased significantly with age (P<0.001). Mean CSF content in studied voxels in the PCC was now 7.4 ± 3.2%. There was a significant linear correlation between age and CSF content (P<0.001, R=0.52). (see fig. 24) A possible J-curve in the CSF fraction can be noted, with a decrease in CSF content during adolescence and an increase from adulthood on. So a polynomial regression of second order was performed (P<0.001, R=0.70). (see fig. 27)

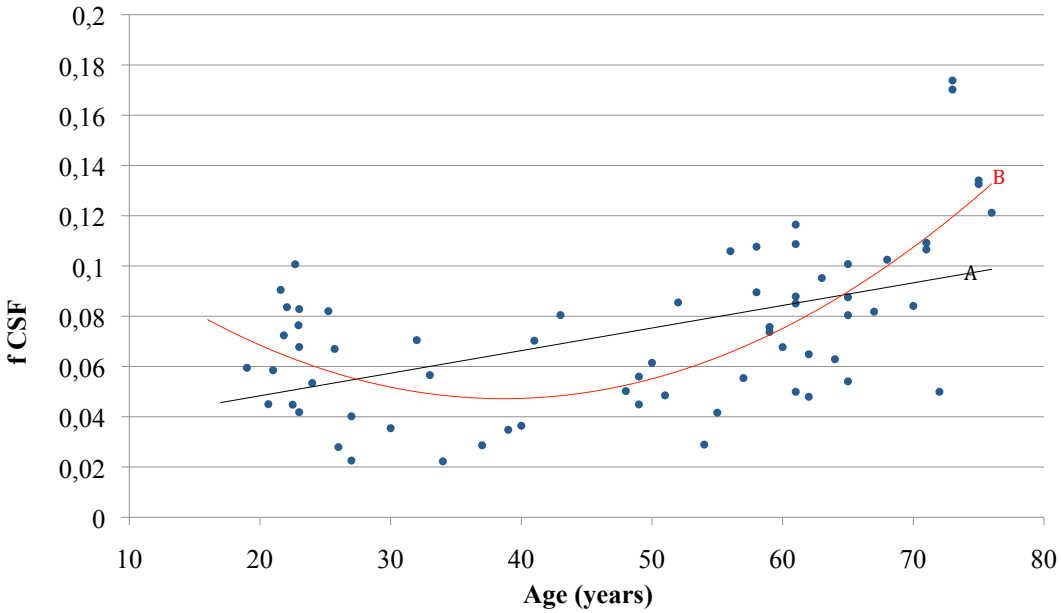

Figure 27 Plot of f_{CSF} vs. age in the PCC. A. Linear regression trend equation: 'f_{CSF} = 0.0009 x age + 0.0304'; correlation coefficient R= 0.52. B. A potential J curve can be noticed, with a peak area in young adults and with old age, so polynomial regression (2nd order) was performed, regression trend: '$f_{CSF} = 6E^{-5}$ x age^2 - 0.0047 x age + 0.1387'; correlation coefficient R= 0.70.

Discussion

NOMARED

Absolute concentration of NAA showed a non-significant increase with age. This contrasts most studies concerning absolute quantification in normal aging. (18, 20, 23, 24, 26) There has long been the belief that normal aging is associated with neuronal loss. When NAA is seen as a neuronal marker (72), the decreased NAA concentrations in these studies could reflect a loss in the number of neurons. Where as two studies showed a significant increase (27, 28), our study found an overall maintained NAA concentration. This could suggest that there is not a measurable loss in neuron numbers with age, or that there is an up-regulation in NAA to maintain functionality. A pathological study showed that the loss in cortical volume with aging was associated with a decrease in neuronal size, not a loss in number of neurons. (7)

NAA/tCr showed a non-significant decrease in the PCC. Taking into account the maintained NAA concentration, this effect should be attributed to an increase in tCr. In explaining changes in metabolite ratios there is always uncertainty, whether the causative factor is the numerator or the denominator. This illustrates the need for absolute quantification in ^{1}H-MRS.

Absolute tCr concentrations and tCr/H_2O ratios were significantly increased in the PCC, in agreement to the abovementioned. These findings illustrate the need for caution when using tCr as an internal metabolite reference, since it is itself sensitive to age-related change. Glial cells appear to be a source of tCr, but not of NAA. (73) Hence, an increase in glial cell number could account for the age-related tCr increase and NAA/tCr decrease. This has been demonstrated in the frontal, temporal and parietal lobes (7) and often corresponds with an increase in Ins, also a marker for gliosis. (74) This concomitant rise in tCr and Ins has been seen in frontal and parietal white matter. (15, 21, 23) This study showed a similar effect in the PCC, but not in the HC, where only a significant increase in Ins with age was seen, without concomitant rise of tCr. This emphasizes the role that both regions play in the development of MCI and Alzheimer's disease and in aging. (50) Indeed, a rise in Ins has also been seen in both brain areas of MCI and Alzheimer patients.

Cho/tCr decreased significantly with age in this study. Caution is advised in analyzing this result, given the age-dependent increase in tCr concentration. However, absolute Cho concentration also showed a decreasing trend, albeit non-significant. Choline can be viewed as a marker for membrane lipid metabolism. (75) Reduced Cho content in the brain could

reflect the loss of myelin lipids. In contrast, most studies demonstrate an in increase in Cho, which could be related to membrane lipid breakdown. (15, 17, 29, 31, 76)

This study has of course its limitations. Firstly tissue segmentation was not performed to correct metabolite concentrations for partial volume effects of gray and white matter. Secondly, because of time limitations, relaxation times for the metabolites could not be attained for each subject. Therefore, corrections for T_1 and T_2 of the metabolite were based on literature values.

MCI

Absolute Cho concentration was found to be increased in MCI patients. These findings could rely on membrane lipid breakdown and inflammatory processes. (76) In other studies, Cho levels have been increased, decreased and unchanged with cognitive decline. (42, 77) These differences could be explained by poor test reproducibility (5, 78). Several studies suggest that Cho levels drop with advanced cognitive decline. (77) A temporary increase in Cho could rely on an increased breakdown of membrane lipids at the start of cognitive decline (i.e. MCI), releasing higher concentrations of Cho. A subsequent fall in Cho levels thus represents further decline. (56)

This study did not show significant differences in NAA levels between healthy subjects and MCI patients. Several studies have shown a decline in NAA levels in the PCC (50, 51, 52, 53) and in the HC. (59) As NAA is a neuronal marker and correlates with atrophy in these regions, these findings could suggest functional losses in neurons. (7, 79)

Ins was not significantly increased in MCI patients compared to control subjects. As shown in the NOMARED study, Ins steadily increases with age. A significantly faster increase in Ins levels has been found in advanced cognitive decline (i.e. Alzheimer's disease). (77) In MCI patients, this increase is probably age-related, rather than pathology-related. (56)

During this study difficulties arose concerning the study subjects. Firstly recruitment was slow, thus explaining the limited subject number in this study. For better comparative statistical research, the study should be continued over a longer period of time.

Identifying and differentiating MCI patients from healthy control subjects proved difficult as well. Control subjects were most often the patients' informants, who accompanied the patients during the diagnostic and research paths. Occasionally, these control subjects proved to suffer from cognitive impairment themselves. This disempowered them as matched control subject to the patient. This also impaired correct diagnosis, since their input that was required in the diagnostic process of the patient, relied on their cognitive well-being. Once the correct diagnosis was established, MCI patients often experienced anxiety during

data acquisition in the MR scanner. Most likely, this can be attributed to their limited grasp on the ongoing events during the experiment. This anxiety affected usability of results because of movement artifacts, or led to cessation of the scan. Clear communication and sufficient time for communication proved vital for successful scan sessions.

Upon looking to the future, the clinical entity of MCI diagnosis could prove to be useful. It provides for early detection of cognitive decline and the potential use of early therapeutic interventions that could halt further impairment. So far no pharmacological interventions were found to be efficacious in MCI. (37) Cognitively stimulating activities, especially during childhood, are thought to be protective against cognitive decline. (36, 42) Nutritional aspects, such as low consumption of saturated fatty acids and cholesterol (41) and sufficient intake of antioxidants, such as vitamins E and C, are associated with less cognitive decline in aging. (47)

MCI as one clinical entity comprise a broad group of cognitive impaired patients, with varying severity. Linking H^1-MRS and other MRI data to neuropsychological test results could prove to be interesting in understanding the pathophysiology of dementia. Already, ^{1}H-MRS results were significantly correlated with MMSE scores. (58, 57, 61)

NOMAREDplus

The combined CSF fractions of NOMARED and NOMAREDplus results did not only show the expected increase of CSF with age, but also a preceding decline of CSF into adulthood. This decrease in CSF fraction could be a representation of increased learning capabilities during young age. In this study lowest CSF fractions can be expected in the range of 35-45 years, using 2nd order polynomial regression. (see fig. 26) There is evidence that age-related cognitive decline accelerates at older age. A study showed that some aspects of age-related cognitive decline, such as memory and general reaction speed, only begin in healthy educated adults when they are in their 20s and 30s. (80) Common believe has always suggested that aging, as a cognition impairing process, doesn't start at birth, but later in life. However, to attain more detailed insight in this evolution, larger scale investigation is needed so as to unravel potentially more complicated correlations.

MRS

MRS is not longer solely used in research, but increasingly in clinical settings as well. Questions on reproducibility of MRS data due to signal-to-noise ratio (SNR), inter operator variability, variability in data analysis and metabolite quantification and signal artifacts. Next

to methodological variation, in vivo metabolic variations are also crucial, for example time of day, consumption of stimulants (caffeine, neuroactive drugs), etc. (81, 82) A study, researching reproducibility, showed that variances in measurements remain under 10%. (76)

MRS remains one of the few non-invasive research tools in several neurological and psychological pathologies. Other options, such as FDG-PET, CT and brain biopsy may provide further pathophysiological insight, but these investigations comprise additional stress for the patient (radiation, invasive procedures, etc.). MRS is extremely safe, if respecting contraindications, and in worst cases, causes symptoms of claustrophobia. With this non-invasive technique there is little to be lost, and lots of information to be gained. MRS data may not yet provide for a conclusive diagnosis in all cases, but when combined with other clinical information it could open diagnostic possibilities for early diagnosis and potential treatment in pathologies such as MCI. Methodological and technical research has provided for ongoing improvements and will most certainly reveal the further potential of the clinical applications of MRS.

Conclusions

Aging is characterized by metabolic increases and declines on the one hand, and metabolic stability on the other. This study indicates a possible gliosis in the aging brain, with a concomitant increase of tCr and Ins in the PCC and an increase of Ins in the HC. The absence of an age-dependent reduction in NAA in the PCC is in contrast to most other studies and may indicate a decrease in neuronal cell size, rather than in cell number. These data may provide a better insight in the differential diagnosis of normal aging and neurodegenerative processes.

MCI patients are of diverse etiology and represent a stage of impairment beyond what is normal for age, but not of sufficient magnitude as to warrant the diagnosis of dementia or Alzheimer's disease. ^{1}H-MRS data may provide further insights in pathophysiology, but large-scale studies are needed.

MCI is often regarded as a single entity, providing for clinical prospects of early diagnosis and treatment. Further research wherein MCI is viewed as a continuous process of cognitive decline, may give rise to correlations between neuropsychological testing scores and severity of cognitive impairment.

MRS has proven to be an interesting tool in neurological and psychological research, without the need for invasive procedures that may stress the patient. Research often refers to metabolite ratios (i.e. relative quantification), but the determination of absolute metabolite concentrations may clarify uncertain changes in brain physiology.

Reference Works:

1. van der Graaf M. In Vivo magnetic resonance spectroscopy: basic methodology and clinical applications. Eur Biophys J. 2010 Mar; 39(4): 527-540.
2. Blink EJ. MRI: Principes. Zoetermeer: MRI-Physics; 2000-2004. Available from: http://mri-physics.net/.
3. Schild HH. MRI made easy (…well almost). Berlin/ Bergkamen: Schering AG; 1990.
4. Hornak JP. The basics of MR. Henietta, NY: Interactive Learning Software; 1996-2010. Available from: http://www.cis.rit.edu/htbooks/mri/index.html.
5. MRI safety [homepage on the Internet]. LA, CA: Shellock R & D Services, Inc.; c2011 [updated 2011; cited 2011, April]. Available from: http://www.mrisafety.com/.
6. Mrak RE, Griffin ST, Graham DI. Aging-associated changes in human brain. J Neuropathol Exp Neurol. 1997; 56(12): 1269-75.
7. Terry RD, DeTeresa R, Hansen LA. Neocortical cell counts in normal human adult aging. Ann Neur. 1987; 21(6): 530-9.
8. O'Sullivan M, Jones DK, Summers PE, Morris RG, Williams SC, Markus HS. Evidence for cortical "disconnection" as a mechanism of age-related cognitive decline. Neurology. 2001; 57(4): 632-8.
9. Sprangler KM, Challa VR, Moody DM, Bell MA. Arteriolar tortuosity of the white matter in aging and hypertension. A microradiographic study. J Neuropathol Exp Neurol. 199'; 53: 22-26.
10. Loessner A, Alavi A, Lewandrowski KU, Mozley D, Souder E, Gur RE. Regional cerebral function determined by FDG-PET in healthy volunteers: normal patterns and changes woth age. J Nucl Med. 1995; 36(7): 1141-9.
11. Hanssen LA, Armstrong DM, Terry RD. An immunohistochemical quantification of fibrous astrocytes in the aging human cerebral cortex. Neurobiol Aging. 1987; 8: 1-6.
12. ShengJ, Mrak RE, Griffin WST: Enlarged and phagocytic, but not primed, IL-1^{+} microglia increase with age in normal human brain. Acta Neuropathol. 1998; 95(3): 229-34.
13. Hof PR, Giannakopoulos P, Bouras C. The neuropathological changes associated with normal brain aging. Histol Histopathol; 1996; 11: 1075-88.
14. Toescu EC. Normal Brain Aging: models and mechanisms. Phil Trans R Soc B. 2005; 360: 2347-54.
15. Chang L, Ernst T, Poland RE, Jenden DJ. In vivo proton magnetic resonance spectroscopy of the normal aging human brain. Life Sci. 1996; 58 (22): 2049-56.

16. Lundbom N, Barnett A, Bonavita S, et al. MR image segmentation and tissue metabolite contrast in ^{1}H spectroscopic imaging of normal and aging brain. Magn Reson Med. 1999; 41 (4): 841-5.
17. Angelie E, Bonmartin A, Boudraa A, Gonnaud PM, Mallet JJ, Sappey-Marinier D. Regional differences and metabolic changes in normal aging of the human brain: proton MR spectroscopic imaging study. ANJR Am J Neuroradiol. 2001; 22 (1): 119-27.
18. Brooks JC, Roberts N, Kemp GJ, Gosney MA, Lye M, Whitehouse GH. A proton magnetic resonance spectroscopy study of age-related changes in frontal lobe metabolite concentrations. Cereb Cortex. 2001; 11 (7): 598-605.
19. Kadota T, Horinouchi T, Kuroda C. Development and aging of the cerebrum: assessment with proton MR spectroscopy. AJNR Am J Neuroradiology. 2001; 22 (1): 125-35.
20. Sailasuta N, Ernst T, Chang L. Regional variations and the effects of age and gender on glutamate concentrations in the human brain. Magn Reson Imaging. 2008; 26 (5): 667-775.
21. Gruber S, Pinker K, Riederer F, et al. Metabolic changes in the normal ageing brain: consistent findings from short and long echo time proton spectroscopy. Eur J Radiol. 2008; 68 (2): 320-7.
22. Fukuzako H, Hashiguchi T, Sakamoto Y, et al. Metabolite changes with age measured by proton magnetic resonance spectroscopy in normal subjects. Psychiatry Clin Neurosci. 1997; 51 (4): 261-3.
23. Chang L, Jiang CS, Ernst T. Effects of age and sex on brain glutamate and other metabolites. Magn Reson Imaging. 2009; 27 (1): 142-5.
24. Raininko R, Mattson P. Metabolite concentrations in supraventricular white matter from teenage to early old age: a short echo time ^{1}H magnetic resonance spectroscopy (MRS) study. Acta Radiol. 2010; 51 (3): 309-15.
25. Grachev ID, Apkarian AV. Aging alters regional multichemical profile of the human brain: an in vivo ^{1}H-MRS study of young versus middle-aged subjects. J Neurochem. 2001; 76 (2): 582-93.
26. Harada M, Miyoshi H, Otsuka H, Nishitani H, Uno M. Mutlivariate analysis of regional metabolic differences in normal ageing on localized quantitative proton MR spectroscopy. Neuroradiology. 2001; 43(6):448-52.
27. Shuff N, Ezekiel F, Gamst AC, et al. Region and tissue differences of metabolites in normally aged brain using multislice ^{1}H magnetic resonance spectroscopic imaging. Magn Reson Med. 2001; 45 (5): 899-907.

28. Charlton RA, Mcintyre DJ, Howe FA, Morris RG, Markus HS. The relationship between white matter brain metabolites and cognition in normal aging: the GENIE study. Brain Re. 2007; 1164: 108-16.
29. Pfefferbaum A, Adalsteinsson E, Spielamn D, Sullivan EV, Lim KO. In vivo spectroscopic quantification of the N-acetyl moiety, creatine, and choline from large volumes of brain gray and white matter: effects of normal aging. Magn reson Med. 1999; 41 (2): 276-84.
30. Saunders DE, Howe FA, van den Boogaart A, Griffiths JR, Brown MM. aging of the adult human brain: in vivo quantification of metabolite content with proton magnetic resonance spectroscopy. J Magn Reson Imaging. 1999; 9 (5): 711-6.
31. Leary SM, Brex PA, MacManus DG, et al. A (1)H magnetic resonance spectroscopy study of aging in parietal white matter: implications for trials in multiple sclerosis. Magn Reson Imaging. 2000; 18 (4): 455-0.
32. Span MM, Ridderinkhof KR, van der Molen MW. Age-related changes in efficiency of cognitive processing across the life span. Acta Psychologica. 2004; 117:155-83.
33. Lim KO, Spielman DM. Estimating NAA in cortical gray matter with applications for measuring changes due to aging. Mang Reson Med. 1997; 37 (3): 372-7.
34. Driscoll I, Hamilton DA, Petropoulos H, et al. The aging Hippocampus: cognitive, biochemical and structural findings. Cereb Cortex. 2003; 13 (12): 1344-51.
35. Szentkuti A, Guderian S, Schiltz K, et al. Quantitative MR analyses of the hippocampus: unspecific metabolic changes in aging. J Neurol. 2004; 251 (11): 1345-53.
36. Peterson RC, Smith GE, Waring SC, Ivnik RJ, Tangalos EG, Kokmen E. Mild cognitive impairment: clinical characterization and outcome. Arch Neurol. 1999; 56 (3): 303-8.
37. Petersen RC, Roberts RO, Knopman DS, Boeve BF, Geda YE, Ivnik RJ, Smith GE, Jack CR. Mild cognitive impairment. Arch Neur. 2009; 66 (12): 1447-55.
38. Petersen RC. Mild cognitive impairment as a diagnostic entity. J Intern Med. 2004; 256: 183-94.
39. Petersen RC, Parisi JE, Dickson DW, et al. Neuropathologic features of amnestic mild cognitive impairment. Arch Neurol; 2006; 63: 665-72.
40. Morris JC. The clinical dementia rating (CDR): current version and scoring rules. Neurology. 1993; 43: 2412-14.
41. Daly E, Zaitchik D, Copeland M, Schmahmann J, Gunther J, Albert M. Predicting conversion to Alzheimer's disease using standardized clinical information. Arch Neurol. 2000; 57: 675-680.

42. Gauthier S, Reisberg B, Zaudig M, et al. International Psychogeriatric Association Expert Conference on mild cognitive impairment. Lancet. 2006; 367: 1262-70.
43. Busse A, Hensel A, Guhne U, Angermeyer MC, Riedel-Heller SG. Mild cognitive impairment: long-term course of four clinical subtypes. Neurology. 2006; 67: 2176-85.
44. Smith CD, Chebrolu H, Wekstein DR, Schmitt FA, Jicha GA, Cooper G, Markesbery WR. Brain structural alterations before mild cognitive impairment. Neurology. 2007; 68: 1268-73.
45. Hansson O, Zetetrberg H, Buchhave P, Londos E, Blennow K, Minthon L. Association between CSF biomarkers and incipient Alzheimer's disease in patients with mild cognitive impairment: a follow-up study. Lancet Neurol. 2006; 5 (3): 228-34.
46. Jack CR Jr, Lowe VJ, Senjem ML, et al. ^{11}C PiB and structural MRI provide complementary information in imaging in Alzheimer's disease and amnestic mild cognitive impairment. Brain. 2008; 131 (3): 665-680.
47. Boeve B, Ferman TJ, Smith GE, et al. Mild cognitive impairment preceding dementia with Lewy bodies. Neurology. 2004; 62 (5): A86.
48. Bennet DA, Schneider JA, Bienas JL, Evans DA, Wilson RS. Mild cognitive impairment is related to Alzheimer disease pathology and cerebral infarctions. Neurology. 2005; 63: 834-41.
49. Markesbery WR. Neuropathologic alterations in mold cognitive impairment: a review. J Alzheimers Dis. 2010; 19 (1): 221-28.
50. Kantarci K, Weigand SD, Petersen RC, Boeve BF, et al. Longitudinal ^{1}H MRS changes in mild cognitive impairment and Alzheimer's disease. Neurobiology of aging. 2007 (28): 1330-39.
51. Pilatus U, Lais C, du Mesnil de Rochemont A, et al. Conversion to dementia in mild cognitive impairment is associated with decline of N-Acetylaspartate and creatine as revealed by magnetic resonance spectroscopy. Psychiatry Research: Neuroimaging. 2009; 173: 1-7.
52. Kantarci K, Weigand SD, Przybelski A, et al. Risk of dementia in MCI: combined effect of cerebrovascular disease, volumetric MRI and ^{1}H MRS. Neurology. 2009; 72: 1519-25.
53. Wang Z, Zhao C, Zhou W, Li K. Regional metabolic changes in the hippocampus and posterior cingulated area detected with 3-tesla magnetic resonance spectroscopy in patients with mild cognitive impairment and Alzheimer disease. Acta Radiol. 2009; 3: 312-9.

54. Kantarci K, Petersen RC, Przybelski A, et al. Hippocampal volumes, proton magnetic resonance spectroscopy metabolites, and cerebrovascular disease in mild cognitive impairment subtypes. Arch Neurol. 2008; 65 (12):1621-8.
55. Li X, Shao X, Wang N, Wang T, Chen G, Zhou H. Correlation of auditory event-related potentials and magnetic resonance spectroscopy measures in mild cognitive impairment. Brain Research. 2010; 1346: 204-212.
56. Chantal S, Braun CM, Bouchard RW, Labelle M, Boulanger Y. Similar ^{1}H magnetic resonance spectroscopic metabolic pattern in the medial temporal lobes of patients with mild cognitive impairment and Alzheimer disease. Brain Research. 2004; 1003: 26-35.
57. Rupsingh R, Borrie M, Smith M, Wells JL, Bartha R. Reduced hippocampal glutamate in Alzheimer disease. Neurobiology of Aging. 2011; 32 (5): 802-10.
58. Zhang B, Ling M, Sun ZZ, Zhu B, Yuan L, Wang Y, Xu Y. Evaluation of functional MRI markers in mild cognitive impairment. J Clinical Neuroscience. 2009 (16): 635-41.
59. Foy CM, Daly EM, Glover A, O'Gorman R, Simmons A, Murphy DG, Lovestone S. Hippocampal proton MR spectroscopy in early Alzheimer's disease and mild cognitive impairment. Brain Topogr. (Epub ahead of print)
60. Garcia Santos JM, Gavrila D, Antunez C, et al. Magnetic resonance spectroscopy performance for detection of dementia, Alzheimer's disease and mild cognitive impairment in a community-based survey. Dement Geriatr Cogn Sisord. 2008; 26: 15-25.
61. Jessen F, Gür O, Block W, et al. A multicenter 1H-MRS study of medial temporal lobe in AD and MCI. Neurology. 2009; 72: 1735-40.
62. Rosenberg SJ, Ryan JJ, Prifitera A. Rey Auditory-Verbal Learning Test performance of patients with and without memory impairment. J Clin Psychology. 1984; 40 (3): 785-7.
63. Ratiney H, Sdika M, Coenradie Y, et al. Time-domain semi-parametric estimation based on a metabolic set. NMR Biomed; 2005; 18: 1-13.
64. Jirù F, Dezortova M, Burian M, Hajek M. The role of relaxation time corrections for the evaluation of long and short echo time 1H MR spectra of the hippocampus by NUMARIS and LCModel techniques. Magma. 2003; 16(3): 135-43.
65. Naressi A, Couturier C, Castang I, de Beer R, Graveron-Demilly D. Java-based graphical user interface for MRUI, a software package for quantitation of in vivo/medical magnetic resonance spectroscopy signals. Computers in Biology and Medicine. 2001; 31: 269-86.

66. Vanhamme L, van den Boogaart A, Van Huffel S. Improved method for accurate and efficient quantification of MRS data with use of prior knowledge. J Magn Reson. 1997; 129: 35-43.
67. Mierisova S, van den Boogaart A, Thac I, et al. New approach for quantitation of short echo time in vivo ^{1}H MR spectra of brain using AMARES.
68. Pijnappel WW, Van den Boogaart A, de beer R, Van Ormondt D. SVD-based quantification of magnetic resonance signals. J Magn Reson. 1992; 97: 122-34.
69. Ernst T, Kreis R, Ross BD. Development of the human brain: in vivo quantification of metabolite and water content with proton magnetic resonance spectroscopy. J Magn Reson. 1993; 30 (4): 424-37.
70. Reyngoudt H, De Deene Y, Descamps B, Paemeleire K, Achten E. ^{1}H-MRS of brain metabolites in migraine without aura: absolute quantification using the phantom replacement technique. Magn Reson Mater Phys. 2010; 4 (23): 227-41.
71. Minati L, Aquino D, Bruzzone MG, Erbetta A. Quantitation of normal metabolite concentrations in six brain regions by in vivo ^{1}H-MR spectroscopy. J Med Phys. 2010; 35 (3): 154-63.
72. Tallan HH. Studies on the distribution of N-acetyl-L-aspartic acid in brain. J Biol Chem. 1956; 224 (1):835-9.
73. Birken DL, Oldendorf WH. N-acetylaspartic acid: a literature review of a compound prominent in ^{1}H-NMR spectroscopic studies of the brain. Neurosci Biobehav Rev. 1989; 13 (1): 23-32.
74. Fisher SK, Novak JE, Agranoff BW. Inositol and higher inositol phosphates in neural tissue: homeostasis, metabolism and functional significance. J Neurochem. 2002; 82 (4): 736-54.
75. Sastry PS. Ipids of nervous tissue: composition and metabolism. Prog Lip Res. 1985; 24 (2): 69-176.
76. Giusto NM, Rocque ME, Ilincheta de Boschero MG. Effect of aging on the content, composition and synthesis of spyngomyelin in the central nervous system. Lipids. 1992; 27 (11): 835-9.
77. Valenzuela MJ, Sachdev D. Magnetic Resonance Spectroscopy in AD. Neurology. 2001; 56: 592-8.
78. Brooks W, Friedman S, Stidley C. Reproducibility oh H1-MRS in vivo. Magn Reson Med. 1999; 41:193-7.
79. Schuff N, Amend DL, Ezekiel F, et al. Change of hippocampal N-acetyl aspartate and volume in Alzheimer's disease. A proton MR spectroscopic imaging and MRI study. Neurology. 1997; 49: 1513-21.

80. Salthouse TA. When does age-related cognitive decline begin? Neurobiology of Aging. 2009; 30: 507-514.
81. Maudsley AA, Domenig C, Sheriff S. Reproducibility of serial whole-brain MR Spectroscopic Imaging. NMR Biomed. 2010; 23: 251-56.
82. Soreni N, Noseworthy MD, Konyer NB, et al. Interindividual, repositioning and time-of-day effects on single voxel proton MR spectroscopy of the anterior cingulated cortex. J Magn Reson Imaging. 2010; 32: 276-282.

Appendices

Article in press: Reyngoudt H, Claeys T, Vlerick L, et al. Age-related differences in metabolites in the posterior cingulate cortex and hippocampus of normal ageing brain: A (1)H-MRS study. Eur J Radiol. 2011 (Epub ahead of print).